

Sivers Function in the Quasi-Classical Approximation

Yuri V. Kovchegov and Matthew D. Sievert

Department of Physics, The Ohio State University, Columbus, OH 43210, USA

September 24, 2018

Abstract

We calculate the Sivers function in semi-inclusive deep inelastic scattering (SIDIS) and in the Drell-Yan process (DY) by employing the quasi-classical Glauber–Mueller/McLerran–Venugopalan approximation. Modeling the hadron as a large “nucleus” with non-zero orbital angular momentum (OAM), we find that its Sivers function receives two dominant contributions: one contribution is due to the OAM, while another one is due to the local Sivers function density in the nucleus. While the latter mechanism, being due to the “lensing” interactions, dominates at large transverse momentum of the produced hadron in SIDIS or of the di-lepton pair in DY, the former (OAM) mechanism is leading in saturation power counting and dominates when the above transverse momenta become of the order of the saturation scale. We show that the OAM channel allows for a particularly simple and intuitive interpretation of the celebrated sign flip between the Sivers functions in SIDIS and DY.

PACS numbers: 12.38.Bx, 13.88.+e, 12.38.Cy, 24.85.+p

1 Introduction

Single transverse spin asymmetries (STSAs) generated in semi-inclusive deep inelastic scattering (SIDIS) and in hadronic collisions are one of the hot topics of research in quantum chromodynamics (QCD), promising unparalleled insight in the physics of chiral symmetry breaking and quark confinement. In the factorization framework involving transverse momentum-dependent distribution functions (TMDs) [1, 2] the origin of STSAs is chiefly ascribed to either the quark TMDs (Sivers effect [3, 4]), to multiple partonic rescattering [5, 6, 7, 8, 9, 10, 11, 12, 13, 14], or to the quark fragmentation functions (Collins effect [15]).

While both the quark TMD and the fragmentation function are non-perturbative, and, according to the conventional wisdom, cannot be calculated from first principles, it is desirable to understand the detailed physical mechanism leading to generation of STSAs in QCD. To that end a significant progress has been achieved by Brodsky, Hwang and Schmidt (BHS) in [10] (see also [16, 5, 6, 7, 9, 11, 17]), where, in a quark–di-quark proton model calculation, it has been shown that the STSA in SIDIS can be generated through an interference of the final-state parton rescattering diagram with the Born-level amplitude. In essence, it was shown in [10, 11] that multiple partonic rescatterings are key to generating the asymmetry. The multiple rescatterings are often referred to as the “lensing” interaction, since, in SIDIS, the associated color-Lorentz force tries to attract the knocked-out quarks back into the hadron [18, 19], thus “focusing” them. The effects of such multiple rescatterings can be absorbed into the Sivers distribution function of a polarized hadron in SIDIS [11, 20].

A consequence of this understanding of the origin of STSA in SIDIS, is that the Sivers function (and, hence, the asymmetry itself) has to change sign between SIDIS and the Drell-Yan process (DY). At the level of the operator matrix element this conclusion has been reached in [11], while an illustration of this result in the BHS model was completed only recently [21] (see also [22] for the outline of the calculation). It is our understanding that in the “lensing” interpretation of STSAs this sign change corresponds to the color-Lorentz force changing sign from attractive to repulsive between a knocked-out quark in SIDIS and the incoming anti-quark in DY.

The goal of the present work is to extend our understanding of the physical mechanism behind the STSA beyond the quark–di-quark model of the proton used in [10, 22, 21] (see [23, 24] for other efforts in a similar direction). In particular, multiple partonic rescatterings in high energy scattering can be particularly simply accounted for in the framework of the quasi-classical approximation to QCD employed in the Glauber–Mueller (GM) [25] and, equivalently, McLerran–Venugopalan (MV) [26, 27, 28] models. In these approaches the hadron is modeled by a large nucleus, with a large number A of nucleons in it. The large number of nucleons leads to high density of small- x gluons in the nuclear wave function, which, in turn, generates a hard scale $Q_s \gg \Lambda_{QCD}$ known as the parton saturation scale, justifying the use of perturbative QCD calculations. (For reviews of the saturation/Color Glass Condensate (CGC) physics see [29, 30, 31, 32, 33].) The fact that the quasi-classical approximation generates a hard scale justifying the approach indicates that it is not simply a “model” of QCD, but, in fact, it represents a limiting behavior of strong interactions at high energy. Multiple rescatterings can be resummed in the GM/MV model as an expansion in powers of the parameter $\alpha_s^2 A^{1/3}$ [34]: the presence of a resummation parameter allows for a controlled approximation to the problem at hand. In the past there was a number of efforts to include spin effects in the saturation/CGC

framework [35, 36, 37, 38, 39, 17, 40, 41].

To alleviate the worry about whether a large nucleus can adequately represent a proton (or any other hadron) in SIDIS and DY experiments, let us point out that in unpolarized scattering the proton may have a significant number of non-perturbatively-generated large- x ($x > 0.01$) partons, which are modeled by “nucleons” in this large-nucleus approximation. The large- x partons/”nucleons”, in turn, give rise to small- x gluons. The resulting expressions for the deep inelastic scattering (DIS) structure functions have been quite successful in describing HERA low- x data [42, 43, 44, 45], also indicating relevance of the large-”nucleus” approximation to the proton wave function at small- x .

In what follows we would have to slightly modify the original MV model of the nucleus by giving the “nucleus” both a non-zero spin and a non-zero orbital angular momentum (OAM). Here this would mean that free nucleons in an approximately spherical bag, as considered originally in [26, 27, 28], would now be polarized and would be orbiting the nuclear spin axis. In a realistic polarized nucleus the nucleons tend to form pairs with zero net OAM, such that the net spin of the nucleus is carried by the few unpaired nucleons and does not get very large (does not grow directly with A). Since it is not clear whether such effect (at the level of quarks and gluons) takes place in the proton we are trying to model, we will not make any particular assumptions about the polarizations and OAMs of the nucleons in our “nucleus”.

The main physical mechanism for generating STSA in the quasi-classical framework is as follows. Imagine a large spinning nucleus. The nucleus is so large that it is almost completely opaque to a colored probe. This strong nuclear shadowing is due to multiple rescatterings in the nucleus generating a short mean free path for the quark, anti-quark, or a gluon.

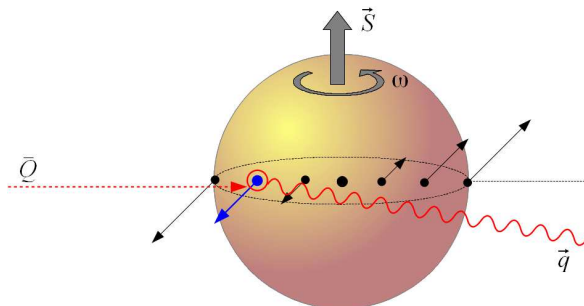


Figure 1: The physical mechanism of STSA in DY as envisioned in the text.

Let us first consider the Drell-Yan process on such a rotating nucleus with shadowing, as shown in Fig. 1 in the nuclear rest frame with the rotation axis of the nucleus perpendicular to the collision axis. The incoming anti-quark (generated in the wave function of the other hadron) scatters on the “front” surface of the polarized nucleus due to the strong shadowing. Since the anti-quark interacts with the nucleons which, at the “front” of the nucleus preferentially rotate with the nucleus out of the plane of the page in Fig. 1, the produced time-like virtual photons are produced preferentially out of the page, generating left-of-polarized-beam single spin asymmetry.¹

¹This mechanism is similar in spirit to the original way of thinking by D. Sivers about the single transverse spin asymmetry. (D. Sivers to M. Sievert, private communications.) A heuristic classical picture of a polarized hadron or nucleus was pioneered in [46].

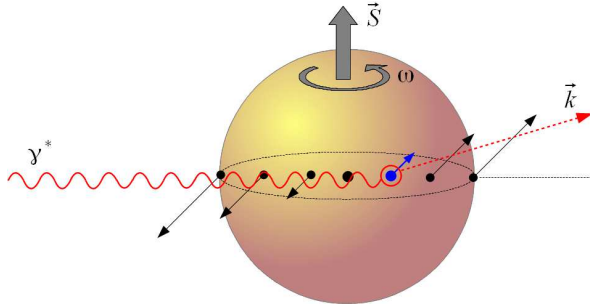


Figure 2: The physical mechanism of STSA in SIDIS as envisioned in the text.

The same mechanism can be applied to generate STSA in SIDIS, as illustrated in Fig. 2, also in the rest frame of the nucleus. Now the incoming virtual photon interacts with the transversely polarized nucleus, producing a quark. For the quark to escape out of the nucleus and be produced the interaction has to take place at the “back” of the nucleus, to minimize the path the quark needs to travel through the nucleus, maximizing its chances to escape. The nucleons in the “back” of the nucleus rotate preferentially into the page of Fig. 2: scattering of a virtual photon on such nucleons results in the right-of-beam single spin asymmetry for the outgoing quarks (quarks produced preferentially with transverse momentum pointing into the page).

Spin asymmetries in DY and SIDIS shown in Figs. 1 and 2 are generated through a combination of OAM effects and nuclear shadowing. The two asymmetries are opposite-sign (left- and right-of-beam), and, assuming that scattering in the two processes happens equal distance from the nuclear edge, are likely to be equal in magnitude, in agreement with the prediction of [11, 22].

As we will see below in the actual calculations, the STSAs in Figs. 1 and 2 do require multiple rescatterings, but they are needed solely to generate nuclear shadowing. Thus the physical mechanism of Figs. 1 and 2 is quite different from the “lensing” interaction [10, 22], in which the knocked-out quark in SIDIS “feels” the net color charge of the remainder of the proton, and is attracted back by this charge [18, 19].² In the presence of shadowing, it would be much harder for the quark in SIDIS to “see” the whole remainder of the polarized proton (nucleus) coherently: thus one expects the “lensing” effect to weaken with increasing shadowing (if we could increase shadowing without modifying the degree of the polarization of the nucleus). This is qualitatively different from the mechanism in Figs. 1 and 2, in which the asymmetry actually increases with shadowing. Clearly, the more opaque the nucleus is, the more likely the interactions to happen at its “front” in DY and at its “back” in SIDIS, making the asymmetry larger.

In the paper below we will outline the calculations leading to the physical picture presented in Figs. 1 and 2. After some generalities in Sec. 2 we proceed in Sec. 3 with the quasi-classical analysis of STSA in SIDIS. As mentioned above, to model the OAM of a polarized nucleus we

²Applying this logic to DY one would expect that to obtain an STSA sign reversal compared to SIDIS one needs the anti-quark in DY to “feel” an equal repulsive force from the rest of proton (that is, from the proton without the quark which is about to annihilate the antiquark): however, it is unclear to us how the incoming anti-quark can “feel” the force of only a part of the intact proton (excluding the quark) while interacting with the whole proton coherently.

have to assume that the nucleus is rotating. This implies a generalization of the original MV and GM models, in which nucleons are static, to include rotational motion of the nucleons. Hence the nucleons need to have both the well-defined positions and momenta: this is only possible in the classical limit. The classical MV model limit is achieved in Sec. 3 using the Wigner functions approach, which allows to specify both the positions and momenta of the nucleons in the polarized nucleus.

We then proceed to the calculation of STSA in SIDIS, identifying two mechanisms for STSA generation: one is due to the coupling of the produced quarks transverse momentum to the OAM of the nucleus, while another one is due to the STSA generated in the scattering of the virtual photon on an individual nucleon along the lines of the BHS mechanism [10] (Sivers function density). The former mechanism is leading in the saturation framework, being dominant in the saturation power counting (for non-zero OAM): it is order-one for $\alpha_s^2 A^{1/3} \sim 1$. The latter mechanism is order- α_s for $\alpha_s^2 A^{1/3} \sim 1$, and is thus subleading.

At large values of the produced quark transverse momentum k_T the OAM mechanism gives the contribution to the Sivers function of the order $A \alpha_s m_N p_T Q_s^2/k_T^6$ with p_T the typical transverse momentum of the valence quarks in the polarized nucleus due to orbital motion and m_N the nucleon mass (with $m_N/3$ roughly the constituent quark mass), while the Sivers function density gives a contribution proportional to $A \alpha_s^2 m_N^2/k_T^4$. Assuming that $p_T \approx m_N$, we see that the Sivers function density mechanism dominates for $k_T > Q_s/\sqrt{\alpha_s}$; conversely, the OAM mechanism is dominant for $k_T < Q_s/\sqrt{\alpha_s}$, the domain including everything inside of the saturation region and a phase-space sector outside of that region.

A similar quasi-classical STSA calculation is carried out for the Drell-Yan process in Sec. 4, where we also explicitly show the mechanism for the sign reversal of the Sivers function outlined in this Introduction. We conclude in Sec. 5 by summarizing our results and outlining possible improvements of our results left for the future work.

2 Definitions: Single Spin Asymmetries, Sivers Function

The single transverse spin asymmetry is defined as

$$A_N(\underline{k}) \equiv \frac{\frac{d\sigma^\uparrow}{d^2k dy} - \frac{d\sigma^\downarrow}{d^2k dy}}{\frac{d\sigma^\uparrow}{d^2k dy} + \frac{d\sigma^\downarrow}{d^2k dy}} = \frac{\frac{d\sigma^\uparrow}{d^2k dy}(\underline{k}) - \frac{d\sigma^\uparrow}{d^2k dy}(-\underline{k})}{\frac{d\sigma^\uparrow}{d^2k dy}(\underline{k}) + \frac{d\sigma^\uparrow}{d^2k dy}(-\underline{k})} \quad (1)$$

for producing a hadron with transverse momentum \underline{k} in SIDIS on a transversely polarized target and in polarized proton-proton collisions or a di-lepton pair with transverse momentum \underline{k} in DY process on a polarized proton. The asymmetry A_N singles out a part of the production cross section proportional to $(\vec{S} \times \vec{p}) \cdot \vec{k}$, where \vec{p} is the 3-momentum of the polarized hadron pointing along the collision axis.

Throughout this paper we will use light-cone coordinates $p^\pm \equiv p^0 \pm p^3$ with the corresponding metric $p \cdot q = \frac{1}{2}p^+q^- + \frac{1}{2}p^-q^+ - \underline{p} \cdot \underline{q}$. Accordingly, we denote four-vectors as $p^\mu = (p^+, p^-, \underline{p})$, with the transverse momentum $\underline{p} \equiv (p^1, p^2)$ and $p_T = p_\perp = |\underline{p}|$.

As we have outline above, a possible physical explanation of the asymmetry is the Sivers effect [3, 4]. The aim of this work is to calculate the Sivers function in the quasi-classical approximation. To define the Sivers function first consider a quark-quark correlation function

in a polarized hadron or nucleus defined by [47, 48]

$$\Phi_{ij}(x, \underline{k}; P, S) \equiv \int \frac{dx^- d^2x_\perp}{2(2\pi)^3} e^{i(\frac{1}{2}xP^+x^- - \underline{x}\cdot\underline{k})} \langle P, S | \bar{\psi}_j(0) \mathcal{U} \psi_i(x^+ = 0, x^-, \underline{x}) | P, S \rangle, \quad (2)$$

where ψ_i is the quark field with Dirac index $i = 1, \dots, 4$, while the quark is taken with transverse momentum \underline{k} and the longitudinal momentum fraction x . The proton (or polarized nucleus) spin four-vector is S^μ , while \mathcal{U} is the gauge link necessary to make the object on the right of Eq. (2) gauge-invariant.

Below, when considering SIDIS and DY, we will work in the light-cone gauge of the projectile. Choosing the polarized proton (nucleus) to move along the light-cone x^+ -direction, such that P^+ is large, we will work in the $A^- = 0$ gauge. In the quasi-classical approximation the $A^- = 0$ gluon field of a large ultrarelativistic nucleus moving along the x^+ -direction has zero transverse component, $\underline{A} = 0$, such that the only non-zero component is A^+ . Defining the Wilson line

$$V_{\underline{x}}[b^-, a^-] \equiv \mathcal{P} \exp \left[\frac{ig}{2} \int_{a^-}^{b^-} dx^- A^+(x^+ = 0, x^-, \underline{x}) \right] \quad (3)$$

we write for the case of SIDIS [11, 20]

$$\mathcal{U}^{SIDIS} = V_{\underline{0}}^\dagger[+\infty, 0] V_{\underline{x}}[+\infty, x^-], \quad (4)$$

while for DY we have

$$\mathcal{U}^{DY} = V_{\underline{0}}[0, -\infty] V_{\underline{x}}^\dagger[x^-, -\infty]. \quad (5)$$

In both cases we neglected the transverse gauge link at $x^- = \pm\infty$ since $\underline{A} = 0$ in the gauge we chose. As will become apparent below, the direction of the Wilson lines in the \mathcal{U} 's is given by the direction of motion of the outgoing quark in SIDIS and the incoming anti-quark in DY. This results in different definitions of the correlator Φ_{ij} for the two processes, which is usually referred to as the controlled process-dependence of the TMDs [11].

The correlation function Φ_{ij} is decomposed as [49, 48]

$$\begin{aligned} \Phi_{ij}(x, \underline{k}; P, S) = & \frac{M}{2P^+} \left[f_1(x, k_T) \frac{\not{P}}{M} + \frac{1}{M^2} f_{1T}^\perp(x, k_T) \epsilon_{\mu\nu\rho\sigma} \gamma^\mu P^\nu k_\perp^\rho S_\perp^\sigma - \frac{1}{M} g_{1s}(x, \underline{k}) \not{P} \gamma^5 \right. \\ & \left. - \frac{1}{M} h_{1T}(x, k_T) i \sigma_{\mu\nu} \gamma^5 S_\perp^\mu P^\nu - \frac{1}{M^2} h_{1s}^\perp(x, \underline{k}) i \sigma_{\mu\nu} \gamma^5 k_\perp^\mu P^\nu + h_1^\perp(x, k_T) \sigma_{\mu\nu} \frac{k_\perp^\mu P^\nu}{M^2} \right]_{ij}, \quad (6) \end{aligned}$$

where M is the mass of the polarized proton or nucleus.

In the following we will be using the Sivers function $f_{1T}^\perp(x, \underline{k})$ and the unpolarized quark TMD $f_1(x, \underline{k})$. These functions can be obtained from the correlator Φ_{ij} using the following expressions

$$\Phi_{ij}(\gamma^+)_{ji} \Big|_{\text{spin independent}} = 2 f_1(x, k_T); \quad (7a)$$

$$\Phi_{ij}(\gamma^+)_{ji} \Big|_{\text{spin dependent}} = \frac{2}{M} \epsilon^{ij} S_\perp^i k_\perp^j f_{1T}^\perp(x, k_T). \quad (7b)$$

3 Semi-Inclusive Deep Inelastic Scattering

We first consider the process of quark production in semi-inclusive deep inelastic lepton scattering on a transversely polarized heavy nucleus: $\ell + A^\uparrow \rightarrow \ell' + q + X$. The leptonic tensor can be factorized out in the usual way, so we represent the process as the scattering of a virtual photon: $\gamma^* + A^\uparrow \rightarrow q + X$. This photon carries a large spacelike virtuality $q_\mu q^\mu = -Q^2$ and knocks out a quark from one of the nucleons, which may then rescatter on the nuclear remnants. The nucleus is taken in the classical GM/MV approximation, which we augment by requiring that the nucleons are polarized and the nucleus rotates around the transverse spin axis, which leads to a non-zero OAM.

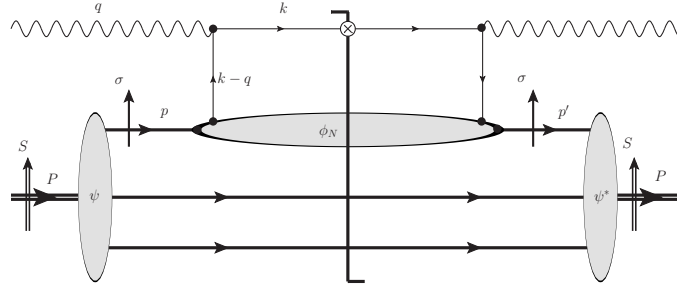


Figure 3: The lowest-order SIDIS process in the usual α_s power-counting. A quark is ejected from a nucleon in the nucleus by the high-virtuality photon, which escapes without rescattering. Different solid horizontal lines represent valence quarks from different nucleons in the nuclear wave function, with the latter denoted by the vertical shaded oval.

Consider first the lowest-order process shown in Fig. 3, in which a quark is ejected without rescattering.³ We work in a frame (such as the photon-nucleus center-of-mass frame) in which the virtual photon moves along the x^- -axis with a large momentum q^- and the nucleus moves along the x^+ -axis with a large momentum P^+ . In this frame, the kinematics are

$$\begin{aligned}
 P^\mu &= \left(P^+, \frac{M_A^2}{P^+}, \underline{0} \right) \\
 q^\mu &= \left(-\frac{Q^2}{q^-}, q^-, \underline{0} \right) \\
 p^\mu &= \left(\alpha P^+, \frac{p_T^2 + m_N^2}{\alpha P^+}, \underline{p} \right) \\
 k^\mu &= \left(\frac{k_T^2}{k^-}, k^-, \underline{k} \right),
 \end{aligned} \tag{8}$$

where M_A is the mass of the nucleus and the on-mass-shell valence quark with momentum p^μ is a part of the light-cone wave function of the nucleus. In what follows we will model nucleons as made out of single valence quarks: in the end of the calculation, to go back to the nucleons

³In small- x physics quark production is dominated by a higher-order in α_s process, where the virtual photon splits into a $q\bar{q}$ pair before hitting the target: since in this work $x = \mathcal{O}(1)$, the dipole process is not dominant, constituting an order- α_s correction to the channel shown in Fig. 3.

one simply would need to replace distribution functions in a valence quark by the distribution functions in the nucleons.

Let us denote the photon-nucleus center-of-mass energy squared by $s_A \equiv (P + q)^2$ and the photon-nucleon (valence quark) center-of-mass energy squared by $\hat{s} \equiv (p + q)^2$. We consider the kinematic limit $s_A \gg \hat{s}, Q^2 \gg p_T^2, k_T^2, M_A^2$ and work to leading order in the small kinematic quantities $\frac{\perp^2}{\hat{s}}, \frac{\perp^2}{Q^2}$, which we denote collectively as $\mathcal{O}(\frac{\perp^2}{Q^2})$. Since we are operating in the limit in which $Q^2 \gg \perp^2 \gg \Lambda^2$, the formalism of TMD factorization applies, justifying the use of the correlator (2) and decomposition (6). Additionally, to a good accuracy one can assume that a typical scale for the momentum fraction α is $\mathcal{O}(1/A)$, where A is the mass number of the nucleus (in fact, $\alpha \approx 1/A$ for the single-valence quark "nucleons" at hand). In this limit,

$$\begin{aligned} p^+ q^- &= \hat{s} + Q^2 \\ q^+ &= - \left(\frac{Q^2}{\hat{s} + Q^2} \right) p^+ = -x p^+ = -\alpha x P^+ \end{aligned} \quad (9)$$

where $x \equiv Q^2/(2p \cdot q)$ is the Bjorken scaling variable per nucleon. The corresponding scaling variable for the entire nucleus is $x_A \equiv Q^2/(2P \cdot q) = \alpha x \approx x/A$. The kinematic limit at hand, $\hat{s} \sim Q^2 \gg p_T^2, k_T^2, M_A^2$ corresponds to $x \sim \mathcal{O}(1)$. The on-shell condition for the outgoing gluon is

$$k^- = \frac{k_T^2}{k^+} = q^- + \frac{p_T^2 + m_N^2}{\alpha P^+} - \frac{(\underline{p} - \underline{k})_T^2}{\alpha P^+ - \alpha x P^+ - k^+} \approx q^- \quad (10)$$

which fixes the struck quark to be ejected along the x^- -direction, so that its light-cone plus momentum

$$k^+ = \frac{k_T^2}{q^-} = \left(\frac{k_T^2}{\hat{s} + Q^2} \right) p^+ = \left(\frac{k_T^2}{Q^2} \right) \alpha x P^+ \quad (11)$$

is small since $\sqrt{\hat{s}} \sim Q \sim p^+ \gg k_T$. This also fixes the momentum fraction of the active quark just before interaction with the photon to be $x_F \equiv (k^+ - q^+)/p^+ \approx -q^+/p^+ = x$ in the usual way. (Note that $q^+ = -Q^2/q^- < 0$.)

In our frame, the x^- -extent of the Lorentz-contracted nucleus is $L^- \sim \frac{M_A}{P^+} R$, where R is the radius of the nucleus in its rest frame. The incoming virtual photon and outgoing quark interact with the nucleus based on their corresponding coherence lengths: $\ell_\gamma^- \sim 1/|q^+|$ and $\ell_k^- \sim 1/k^+$, respectively. Comparing these to the size of the nucleus,

$$\begin{aligned} \frac{\ell_\gamma^-}{L^-} &\sim \frac{1}{x} \frac{1}{\alpha M_A R} \sim \mathcal{O}(A^{-1/3}) \ll 1, \\ \frac{\ell_k^-}{L^-} &\sim \frac{1}{x} \left(\frac{Q^2}{k_T^2} \right) \frac{1}{\alpha M_A R} \sim \mathcal{O} \left(\frac{Q^2 + \hat{s}}{\perp^2} A^{-1/3} \right) \gg 1, \end{aligned} \quad (12)$$

we see that the photon's coherence length is short, but the coherence length of the ejected quark is parametrically large for $\hat{s}, Q^2 \gg \perp^2 A^{1/3}$. Thus, for our calculation in which $x \sim \mathcal{O}(1)$, the virtual photon interacts incoherently (locally) on a single nucleon, but the ejected quark interacts coherently with all of the remaining nucleons it encounters before escaping the nucleus.

This limit thus combines the local “knockout” picture of the deep inelastic scattering process with the coherent rescattering that usually characterizes the small- x limit. In the formal limit of a large nucleus in which $\alpha_s \ll 1$ and $A \gg 1$ such that $\alpha_s^2 A^{1/3} \sim \mathcal{O}(1)$, these coherent interactions with subsequent nucleons must be re-summed according to this saturation-based power counting.

3.1 Quark Production in SIDIS

In general it is rather straightforward to write an answer for the quasi-classical quark production in SIDIS. As we mentioned in the Introduction, here the problem is a little more subtle than usual since we are interested in also including transverse and longitudinal motion of the nucleons in the nucleus in order to model its OAM. Thus our quasi-classical description of the nucleus has to provide us both with the positions and momenta of the nucleons. This can be done using Wigner distributions.

Let us illustrate the method with a simple single-rescattering process from Fig. 3. Just like in the parton model, the time scale of inter-nucleon interactions is Lorentz-dilated in the infinite momentum frame of the nucleus that we are working in. We can, therefore, write the scattering amplitude for the process in Fig. 3 as a product of the light-cone wave function ψ of the valence quarks in the nucleus (defined according to light-front perturbation theory rules [50, 51] in the boost-invariant convention of [33]) with the quark–virtual photon scattering amplitude M_K :

$$M_{tot} = \psi(p) M_K(p, q, k). \quad (13)$$

Here $\psi(p) = \psi(p^+/P^+, \underline{p})$ is the boost-invariant light-cone wave function of a valence quark (in one of the nucleons) in the nucleus, while M_K is the scattering amplitude for the “knock-out” process $\gamma^* + q \rightarrow q + X$. The sum over valence quark spin and color is implied in (13). In calculating the quark production process we need to square this amplitude, integrate it over the momentum of the final state gluon and sum over all nucleons in the nucleus. Since momenta k and q are fixed, this amounts to integrating over p . One gets

$$\int \frac{dp^+ d^2p}{2(p^+ + q^+) (2\pi)^3} |M_{tot}|^2 = A \int \frac{dp^+ d^2p}{2(p^+ + q^+) (2\pi)^3} |\psi(p)|^2 |M_K(p, q, k)|^2. \quad (14)$$

First let us introduce a Fourier transform of the valence quark wave function,

$$\psi(b) \equiv \psi(b^-, \underline{b}) = \int \frac{dp^+ d^2p}{2\sqrt{p^+} (2\pi)^3} e^{-ip \cdot b} \psi(p), \quad (15)$$

with $p \cdot b = \frac{1}{2} p^+ b^- - \underline{p} \cdot \underline{b}$. Next we define the Wigner distribution for the valence quarks (which is closely related to the Wigner distribution of the nucleons in the quasi-classical MV model employed here) with the help of the Fourier transform (15):

$$W(p, b) \equiv W(p^+, \underline{p}; b^-, \underline{b}) \equiv \int d^2\delta b d\delta b^- e^{ip \cdot \delta b} \psi(b + \frac{1}{2}\delta b) \psi^*(b - \frac{1}{2}\delta b). \quad (16)$$

Note that the wave function is normalized such that

$$\int \frac{dp^+ d^2p}{2p^+ (2\pi)^3} |\psi(p)|^2 = 1 \quad (17)$$

giving

$$\int \frac{dp^+ d^2p db^- d^2b}{2(2\pi)^3} W(p, b) = 1. \quad (18)$$

Since

$$\int d^2b db^- W(p, b) = |\psi(p)|^2/p^+ \quad (19)$$

we can recast Eq. (14) as

$$\int \frac{dp^+ d^2p}{2(p^+ + q^+) (2\pi)^3} |M_{tot}|^2 = A \int \frac{dp^+ d^2p db^- d^2b}{2(2\pi)^3} W(p, b) \frac{p^+}{p^+ + q^+} |M_K(p, q, k)|^2. \quad (20)$$

Finally, in the following, as usual in the saturation framework, it would be convenient to calculate the scattering amplitude in (partial) transverse coordinate space. Writing

$$M_K(p, q, k) = \int d^2x e^{-i\mathbf{k}\cdot(\mathbf{x}-\mathbf{b})} M_K(p, q, \mathbf{x} - \mathbf{b}) \quad (21)$$

(with k^- and k^+ fixed by Eqs. (10) and (11)) we rewrite Eq. (20) as

$$\begin{aligned} \int \frac{dp^+ d^2p}{2(p^+ + q^+) (2\pi)^3} |M_{tot}|^2 &= A \int \frac{dp^+ d^2p db^- d^2b}{2(2\pi)^3} W(p, b) \frac{p^+}{p^+ + q^+} \\ &\times \int d^2x d^2y e^{-i\mathbf{k}\cdot(\mathbf{x}-\mathbf{y})} M_K(p, q, \mathbf{x} - \mathbf{b}) M_K^*(p, q, \mathbf{y} - \mathbf{b}). \end{aligned} \quad (22)$$

Note that the Fourier transform (21) appears to imply that \underline{b} is the transverse position of the outgoing gluon in Fig. 3, whereas in the Wigner distribution \underline{b} is the position of the valence quark p . As we will shortly see such interpretation is not inconsistent: in the classical limit of a large nucleus the Wigner distribution is a slowly varying function of \underline{b} , with changes in W becoming significant over the variations of \underline{b} over distances of the order of nucleon size 1 fm or larger. The valence quark and outgoing gluon in Fig. 3 are perturbatively close to each other (being the part of the same Feynman diagram), and hence the difference in their positions is outside the precision of $W(p, b)$ and can be taken to be the same in the Wigner distribution.

In Appendix A we show that the formula (22) holds not only at the lowest order, but when multiple rescatterings are included as well, such that in the kinematics outlined above

$$\begin{aligned} \int \frac{dp^+ d^2p}{2(p^+ + q^+) (2\pi)^3} |A_{tot}|^2 &= A \int \frac{dp^+ d^2p db^- d^2b}{2(2\pi)^3} W(p, b) \frac{p^+}{p^+ + q^+} \\ &\times \int d^2x d^2y e^{-i\mathbf{k}\cdot(\mathbf{x}-\mathbf{y})} A(p, q, \mathbf{x} - \mathbf{b}) A^*(p, q, \mathbf{y} - \mathbf{b}), \end{aligned} \quad (23)$$

where we define the energy-independent (at the lowest non-trivial order) $2 \rightarrow 2$ scattering amplitudes by (see also Eqs. (A8) and (A11)) [33]

$$A(p, q, k) = \frac{M(p, q, k)}{2p^+ q^-} \quad (24)$$

and $A(p, q, k)$ in Eq. (23) denotes the sum over rescatterings of the virtual photon on any number of nucleons in the nucleus.⁴ (Note that for a “nucleus” made out of a single nucleon $p^+ = P^+$, which allows one to reduce Eq. (22) to Eq. (23) by neglecting the “spectator” nucleons.) We therefore conclude that the quark production cross section for the $\gamma^* + A \rightarrow q + X$ process can be written as

$$\frac{d\sigma^{\gamma^*+A \rightarrow q+X}}{d^2k dy} = A \int \frac{dp^+ d^2p db^- d^2b}{2(2\pi)^3} W(p, b) \frac{d\hat{\sigma}^{\gamma^*+NN\dots N \rightarrow q+X}}{d^2k dy}, \quad (25)$$

where the cross section for producing a quark in γ^* scattering on the nucleons is

$$\frac{d\hat{\sigma}^{\gamma^*+NN\dots N \rightarrow q+X}}{d^2k dy} = \mathcal{N} \int d^2x d^2y e^{-i\mathbf{k}\cdot(\mathbf{x}-\mathbf{y})} A_K(p, q, \mathbf{x} - \mathbf{b}) A_K^*(p, q, \mathbf{y} - \mathbf{b}) D_{\mathbf{x}\mathbf{y}}[+\infty, b^-] \quad (26)$$

with the semi-infinite fundamental dipole scattering amplitude given by (cf. Eq. (4))

$$D_{\mathbf{x}\mathbf{y}}[+\infty, b^-] = \left\langle \frac{1}{N_c} \text{Tr} \left[V_{\mathbf{x}}[+\infty, b^-] V_{\mathbf{y}}^\dagger[+\infty, b^-] \right] \right\rangle \quad (27)$$

and with some \hat{s} and Q^2 -dependent prefactor \mathcal{N} . Here $y = \ln 1/x$ is the rapidity of the produced quark and a factor of A in Eq. (25) accounts for the fact that the first scattering can take place on any of the A nucleons. We fixed the normalization of Eq. (25) by requiring it to be valid for a nucleus made out of a single nucleon, which would be described by a trivial Wigner distribution fixing the momentum and position of the nucleon by simple delta-functions. (Alternatively one could require the formula to be valid for the case of cross section $\hat{\sigma}$ independent of p and b .)

As already mentioned before, with the accuracy of the large- A classical approximation, the argument \mathbf{b} in the Wigner distribution can be replaced by any other transverse coordinate involved in the scattering process. Hence one can replace \mathbf{b} in $W(b, p)$ from Eq. (25) by either \mathbf{x} or \mathbf{y} from Eq. (26), or by any linear combination of those variables. Replacing \mathbf{b} in $W(b, p)$ from Eq. (25) by $(\mathbf{x} + \mathbf{y})/2$ and employing Eq. (26) we write

$$\begin{aligned} \frac{d\sigma^{\gamma^*+A \rightarrow q+X}}{d^2k dy} &= A \int \frac{dp^+ d^2p db^-}{2(2\pi)^3} \int d^2x d^2y W\left(p, b^-, \frac{\mathbf{x} + \mathbf{y}}{2}\right) \\ &\times e^{-i\mathbf{k}\cdot(\mathbf{x}-\mathbf{y})} |A_K|^2(p, q, \mathbf{x} - \mathbf{y}) D_{\mathbf{x}\mathbf{y}}[+\infty, b^-], \end{aligned} \quad (28)$$

where

$$\begin{aligned} |A_K|^2(p, q, \mathbf{x} - \mathbf{y}) &\equiv \mathcal{N} \int d^2b A_K(p, q, \mathbf{x} - \mathbf{b}) A_K^*(p, q, \mathbf{y} - \mathbf{b}) \\ &= \int \frac{d^2k'}{(2\pi)^2} e^{i\mathbf{k}'\cdot(\mathbf{x}-\mathbf{y})} \frac{d\hat{\sigma}^{\gamma^*+N \rightarrow q+X}}{d^2k' dy}(p, q). \end{aligned} \quad (29)$$

Substituting Eq. (29) into Eq. (28) yields

$$\begin{aligned} \frac{d\sigma^{\gamma^*+A \rightarrow q+X}}{d^2k dy} &= A \int \frac{dp^+ d^2p db^-}{2(2\pi)^3} \int d^2x d^2y W\left(p, b^-, \frac{\mathbf{x} + \mathbf{y}}{2}\right) \\ &\times \int \frac{d^2k'}{(2\pi)^2} e^{-i(\mathbf{k}-\mathbf{k}')\cdot(\mathbf{x}-\mathbf{y})} \frac{d\hat{\sigma}^{\gamma^*+N \rightarrow q+X}}{d^2k' dy}(p, q) D_{\mathbf{x}\mathbf{y}}[+\infty, b^-]. \end{aligned} \quad (30)$$

⁴Strictly-speaking we need to include in Eq. (23) Wigner function convolutions with the all the interacting nucleons in the nucleus: however, since in our kinematics only the first “knockout” process depends on the transverse momentum p_\perp of the nucleon, we only keep one convolution with the Wigner function explicitly.

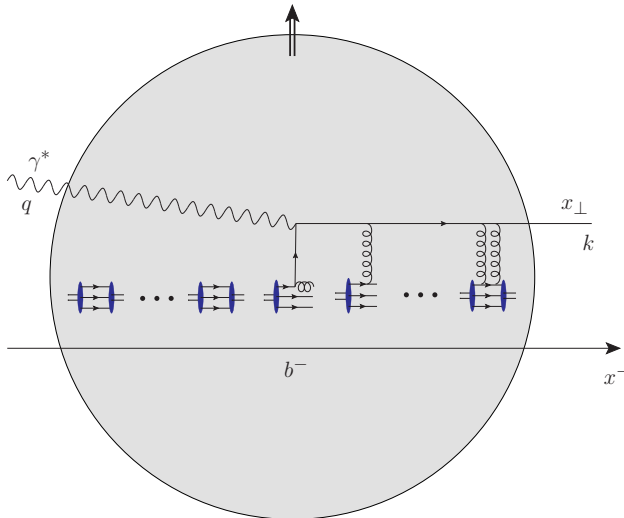


Figure 4: Space-time structure of quark production in the quasi-classical SIDIS process in the rest frame of the nucleus, overlaid with one of the corresponding Feynman diagrams. The shaded circle is the transversely polarized nucleus, with the vertical double arrow denoting the spin direction.

Eq. (30) is our starting point for exploring the STSA in SIDIS: it gives the quark production cross section in the quasi-classical approximation.

The expression (30) is illustrated in Fig. 4: the first interaction between the incident virtual photon and a nucleon in the transversely polarized nucleus happens at the longitudinal coordinate b^- . A quark is knocked out, which proceeds to interact with the rest of the nucleons in the nucleus. This latter interaction is recoilless and is encoded in a Wilson line.

The Wigner distribution in Eq. (30) allows to take the quasi-classical GM/MV limit of a large nucleus in a controlled way. For a large "classical" nucleus we usually can replace $W(p, b)$ by the following classical expression for it (neglecting longitudinal orbital motion of the nucleons)

$$W_{cl}(p, b) = \frac{4\pi}{A} \rho(\underline{b}, b^-) \delta\left(p^+ - \frac{P^+}{A}\right) w(\underline{p}, b), \quad (31)$$

where $\rho(\underline{b}, b^-)$ is the nucleon number density normalized such that

$$\int d^2b db^- \rho(\underline{b}, b^-) = A. \quad (32)$$

The function $w(\underline{p}, b)$ in Eq. (31) is responsible for the transverse momentum distribution of the nucleons and, to satisfy Eq. (18), is normalized such that

$$\int \frac{d^2p}{(2\pi)^2} w(\underline{p}, b) = 1. \quad (33)$$

As originally formulated [26, 27, 28], the MV model contained no dependence on the spin or transverse momentum of the valence quarks. This result is recovered by using $w_{MV} = (2\pi)^2 \delta^2(\underline{p})$.

Substituting the classical Wigner distribution (31) into Eq. (30) yields

$$\begin{aligned} \frac{d\sigma^{\gamma^*+A\rightarrow q+X}}{d^2k dy} &= \int \frac{d^2p db^-}{(2\pi)^2} d^2x d^2y \rho\left(\frac{\underline{x}+\underline{y}}{2}, b^-\right) w\left(\underline{p}, \frac{\underline{x}+\underline{y}}{2}, b^-\right) \\ &\times \int \frac{d^2k'}{(2\pi)^2} e^{-i(\underline{k}-\underline{k}')\cdot(\underline{x}-\underline{y})} \frac{d\hat{\sigma}^{\gamma^*+N\rightarrow q+X}}{d^2k' dy}(p, q) D_{\underline{x}\underline{y}}[+\infty, b^-], \end{aligned} \quad (34)$$

which is a simplified version of Eq. (30).

3.2 Quasi-Classical Sivers Function in SIDIS

Imagine a large nucleus with the total spin \vec{J} such that

$$\vec{J} = \vec{L} + \vec{S}, \quad (35)$$

where \vec{L} is the OAM of all the nucleons in the nucleus and \vec{S} is the net spin of all the nucleons. In the quasi-classical approximation at hand the OAM is generated by rotation of the nucleons around a preferred axis. The nucleus is transversely polarized to the beam: we assume that both \vec{L} and \vec{S} point along the (positive or negative) \hat{x} -axis.

The result (30) for the quark production cross section in SIDIS can be utilized to write down an expression for SIDIS Sivers function of the large nucleus with the help of Eq. (7b). We first note that the quark production cross section in SIDIS is proportional to the correlator (2) with the future-pointing Wilson line given by Eq. (4) (cf. Eqs. (26) and (27)). The gauge link in (27) begins and ends at the same b^- , while the more general gauge link in (4) has different endpoints at 0 and x^- . The reason is that the nuclear wave function is composed of color-neutral ‘‘nucleons’’ localized in b^- ; hence there is only a contribution to the correlator when the gauge link both begins and ends at the same b^- . The Dirac γ^+ -matrix of Eq. (7b) is also present in the quark production cross section since the Dirac structure of the large- k^- outgoing quark line is given by $\gamma^+ k^-$. To obtain the Sivers function one only needs to eliminate the gamma-matrices stemming from the quark-photon vertices in the amplitude and in the complex conjugate amplitude; this can be done by simply contracting the Lorentz indices of these gamma-matrices [21]. While such contraction is not allowed in a calculation of the SIDIS cross section due to non-trivial structure of the lepton tensor, it is a legitimate method of extracting the Sivers function [21], since $\gamma_\mu \gamma^+ \gamma^\mu = -2\gamma^+$. We thus see that an equation like (30) would still hold for $\text{Tr}[\Phi \gamma^+]$ instead of SIDIS cross section, since to obtain the former one simply needs to repeat all the steps of the cross section derivation that led to Eq. (30) without inserting the photon polarizations (implicit in (30)), and adding a contraction over Lorentz indices of the gamma-matrices from the quark-photon vertices in the end.

By analogy with Eq. (30) we can express the quark correlation function Φ_A of the nucleus in terms of the quasi-classical distribution $W_N(p, b)$ of nucleons, the quark correlators ϕ_N of individual nucleons, and the semi-infinite Wilson line trace $D_{\underline{x}\underline{y}}[+\infty, b^-]$:

$$\begin{aligned} \text{Tr}[\Phi_A(\bar{x}, \underline{k}; P, J) \gamma^+] &= A \int \frac{dp^+ d^2p db^-}{2(2\pi)^3} d^2x d^2y \sum_{\sigma} W_N^{\sigma} \left(p, b^-, \frac{\underline{x}+\underline{y}}{2} \right) \int \frac{d^2k'}{(2\pi)^2} e^{-i(\underline{k}-\underline{k}')\cdot(\underline{x}-\underline{y})} \\ &\times \text{Tr}[\phi_N(x, \underline{k}' - x \underline{p}; p, \sigma) \gamma^+] D_{\underline{x}\underline{y}}[+\infty, b^-]. \end{aligned} \quad (36)$$

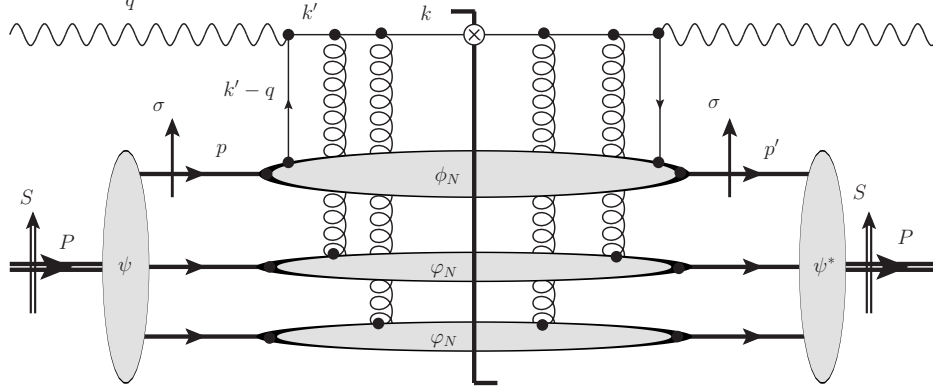


Figure 5: Decomposition of the nuclear quark distribution Φ_A probed by the SIDIS virtual photon into mean-field wave functions ψ, ψ^* of nucleons and the quark and gluon distributions ϕ_N and φ_N of the nucleons.

Eq. (36) is illustrated in Fig. 5. In Eq. (36) we explicitly show the sum over the polarizations $\sigma = \pm 1/2$ of the nucleons along the x -axis. Note that $x = -q^+/p^+$ and it varies with p^+ inside the integral; at the same time the “averaged” value of Bjorken- x per nucleon is $\bar{x} = -A q^+/P^+$. The quark correlator of the nucleus Φ_A is defined by Eq. (2),

$$\Phi_{ij}^A(\bar{x}, \underline{k}; P, J) \equiv \int \frac{dx^- d^2x_\perp}{2(2\pi)^3} e^{i(\frac{1}{2}\bar{x}P^+x^- - \underline{x}\cdot\underline{k})} \langle A; P, J | \bar{\psi}_j(0) \mathcal{U}^{SIDIS} \psi_i(x^+ = 0, x^-, \underline{x}) | A; P, J \rangle, \quad (37)$$

along with the corresponding nucleonic correlator is

$$\phi_{ij}^N(x, \underline{k}; p, \sigma) \equiv \int \frac{dx^- d^2x_\perp}{2(2\pi)^3} e^{i(\frac{1}{2}x p^+ x^- - \underline{x}\cdot\underline{k})} \langle N; p, \sigma | \bar{\psi}_j(0) \mathcal{U}^{SIDIS} \psi_i(x^+ = 0, x^-, \underline{x}) | N; p, \sigma \rangle. \quad (38)$$

These definitions are done in a frame in which the parent particle’s transverse momentum is zero. The $\underline{k}' - x \underline{p}$ in the argument of ϕ_N in Eq. (36) is obtained by making a transverse boost from the frame in which the nucleon has transverse momentum \underline{p} into a frame in which $\underline{p} = \underline{0}$ (and the definition (38) applies). Note that our lab frame corresponds to the photon-nucleus center-of-mass frame in which $\underline{q} = \underline{P} = \underline{0}$. The polarization-dependent Wigner functions are normalized as (cf. Eq. (18))

$$\begin{aligned} \int \frac{dp^+ d^2p db^- d^2b}{2(2\pi)^3} A W^{+1/2}(p, b) &= \# \text{ spin-up nucleons}; \\ \int \frac{dp^+ d^2p db^- d^2b}{2(2\pi)^3} A W^{-1/2}(p, b) &= \# \text{ spin-down nucleons}. \end{aligned} \quad (39)$$

As in [48], the correlation functions in Eq. (36) can be parametrized in terms of the TMD distribution functions, of which the most relevant to the problem at hand are the unpolarized

distribution f_1 and the Sivers function f_{1T}^\perp . Using Eqs. (7) we write

$$\text{Tr}[\Phi_A(\bar{x}, \underline{k}; P, J) \gamma^+] = 2 f_1^A(\bar{x}, k_T) + \frac{2}{M_A} \hat{z} \cdot (\underline{J} \times \underline{k}) f_{1T}^{\perp A}(\bar{x}, k_T) \quad (40a)$$

$$\begin{aligned} \text{Tr}[\phi_N(x, \underline{k}' - x \underline{p}; p, \sigma) \gamma^+] &= 2 f_1^N(x, |\underline{k}' - x \underline{p}|) + \\ &+ \frac{2}{m_N} \hat{z} \cdot (\underline{\sigma} \times (\underline{k}' - x \underline{p})) f_{1T}^{\perp N}(x, |\underline{k}' - x \underline{p}|), \end{aligned} \quad (40b)$$

where we introduced the unpolarized quark TMDs (f_1^A and f_1^N) and Sivers functions ($f_{1T}^{\perp A}$ and $f_{1T}^{\perp N}$) for the nucleus and nucleons respectively, along with the masses M_A and m_N of the nucleus and nucleons.

We may extract the Sivers function of the nucleus $f_{1T}^{\perp A}$ by antisymmetrizing (40a) with respect to either the nuclear spin or the momentum \underline{k} of the produced quark.⁵

$$\hat{z} \cdot (\underline{J} \times \underline{k}) f_{1T}^{\perp A}(\bar{x}, k_T) = \frac{1}{4} M_A \text{Tr}[\Phi_A(\bar{x}, \underline{k}; P, J) \gamma^+] - (\underline{k} \rightarrow -\underline{k}). \quad (41)$$

Using Eq. (36) in Eq. (41) we write

$$\begin{aligned} \hat{z} \cdot (\underline{J} \times \underline{k}) f_{1T}^{\perp A}(\bar{x}, k_T) &= \frac{1}{4} M_A A \int \frac{dp^+ d^2 p db^-}{2(2\pi)^3} d^2 x d^2 y \sum_\sigma W_N^\sigma \left(p, b^-, \frac{x+y}{2} \right) \\ &\times \int \frac{d^2 k'}{(2\pi)^2} e^{-i(\underline{k}-\underline{k}') \cdot (\underline{x}-\underline{y})} \text{Tr}[\phi_N(x, \underline{k}' - x \underline{p}; p, \sigma) \gamma^+] D_{\underline{x}\underline{y}}[+\infty, b^-] - (\underline{k} \rightarrow -\underline{k}). \end{aligned} \quad (42)$$

We can decompose the quark correlator in a nucleon ϕ_N into the nucleon's unpolarized quark distribution f_1^N and Sivers function $f_{1T}^{\perp N}$ using (40b). Substituting this into Eq. (42) yields

$$\begin{aligned} \hat{z} \cdot (\underline{J} \times \underline{k}) f_{1T}^{\perp A}(\bar{x}, k_T) &= \frac{1}{4} M_A A \int \frac{dp^+ d^2 p db^-}{2(2\pi)^3} d^2 x d^2 y \sum_\sigma W_N^\sigma \left(p, b^-, \frac{x+y}{2} \right) \int \frac{d^2 k'}{(2\pi)^2} \\ &\times e^{-i(\underline{k}-\underline{k}') \cdot (\underline{x}-\underline{y})} \left[2 f_1^N(x, |\underline{k}' - x \underline{p}|) + \frac{2}{m_N} \hat{z} \cdot (\underline{\sigma} \times (\underline{k}' - x \underline{p})) f_{1T}^{\perp N}(x, |\underline{k}' - x \underline{p}|) \right] \\ &\times D_{\underline{x}\underline{y}}[+\infty, b^-] - (\underline{k} \rightarrow -\underline{k}). \end{aligned} \quad (43)$$

We can understand the sources of the T -odd nuclear Sivers function $f_{1T}^{\perp A}$ by explicitly (anti)symmetrizing the various terms on the right of Eq. (43). To start with, perform the nucleon spin sum \sum_σ in a basis parallel or antiparallel to the nuclear spin \underline{S} . This can be done using the definitions

$$\begin{aligned} \sum_\sigma W_N^\sigma(p, b) &\equiv W_{unp}(p, b) \\ \sum_\sigma W_N^\sigma(p, b) \underline{\sigma} &\equiv \frac{1}{A} W_{trans}(p, b) \underline{S}, \end{aligned} \quad (44)$$

⁵In doing so we assume that the Sivers function is an even function of \underline{k} , which is indeed the case due to its T -symmetry properties.

where we will refer to W_{unp} as the distribution of unpolarized nucleons and to W_{trans} as the nucleon transversity distribution. Note that

$$\int \frac{dp^+ d^2p db^- d^2b}{2(2\pi)^3} W_{unp}(p, b) = 1, \quad \int \frac{dp^+ d^2p db^- d^2b}{2(2\pi)^3} W_{trans}(p, b) = 1, \quad (45)$$

as follows from the definition (44) and from (39).

Eq. (43) becomes

$$\begin{aligned} \hat{z} \cdot (\underline{J} \times \underline{k}) f_{1T}^{\perp A}(\bar{x}, k_T) &= \frac{M_A}{2} \int \frac{dp^+ d^2p db^-}{2(2\pi)^3} d^2x d^2y \frac{d^2k'}{(2\pi)^2} e^{-i(\underline{k}-\underline{k}') \cdot (\underline{x}-\underline{y})} \left[A W_{unp} \left(p, b^-, \frac{\underline{x} + \underline{y}}{2} \right) \right. \\ &\times f_1^N(x, |\underline{k}' - x \underline{p}|) + W_{trans} \left(p, b^-, \frac{\underline{x} + \underline{y}}{2} \right) \frac{1}{m_N} \hat{z} \cdot (\underline{S} \times (\underline{k}' - x \underline{p})) f_{1T}^{\perp N}(x, |\underline{k}' - x \underline{p}|) \left. \right] \\ &\times D_{\underline{xy}}[+\infty, b^-] - (\underline{k} \rightarrow -\underline{k}). \end{aligned} \quad (46)$$

Now, in the terms with $(\underline{k} \rightarrow -\underline{k})$ being subtracted, we also redefine the dummy integration variables $\underline{x} \leftrightarrow \underline{y}$, $\underline{k}' \rightarrow -\underline{k}'$, and $\underline{p} \rightarrow -\underline{p}$. This leaves the Fourier factors and the distribution functions f_1^N , $f_{1T}^{\perp N}$ unchanged, giving

$$\begin{aligned} \hat{z} \cdot (\underline{J} \times \underline{k}) f_{1T}^{\perp A}(\bar{x}, k_T) &= \frac{M_A}{2} \int \frac{dp^+ d^2p db^-}{2(2\pi)^3} d^2x d^2y \frac{d^2k'}{(2\pi)^2} e^{-i(\underline{k}-\underline{k}') \cdot (\underline{x}-\underline{y})} \left\{ f_1^N(x, |\underline{k}' - x \underline{p}|) \right. \\ &\times A \left[W_{unp} \left(p^+, \underline{p}, b^-, \frac{\underline{x} + \underline{y}}{2} \right) D_{\underline{xy}}[+\infty, b^-] - W_{unp} \left(p^+, -\underline{p}, b^-, \frac{\underline{x} + \underline{y}}{2} \right) D_{\underline{yx}}[+\infty, b^-] \right] \\ &+ \frac{1}{m_N} \hat{z} \cdot (\underline{S} \times (\underline{k}' - x \underline{p})) f_{1T}^{\perp N}(x, |\underline{k}' - x \underline{p}|) \\ &\times \left[W_{trans} \left(p^+, \underline{p}, b^-, \frac{\underline{x} + \underline{y}}{2} \right) D_{\underline{xy}}[+\infty, b^-] + W_{trans} \left(p^+, -\underline{p}, b^-, \frac{\underline{x} + \underline{y}}{2} \right) D_{\underline{yx}}[+\infty, b^-] \right] \left. \right\}. \end{aligned} \quad (47)$$

At this point it is convenient to explicitly (anti)symmetrize the distribution functions with respect to $\underline{p} \leftrightarrow -\underline{p}$ and the Wilson lines with respect to $\underline{x} \leftrightarrow \underline{y}$. Define

$$\begin{aligned} S_{\underline{xy}} &\equiv \frac{1}{2}(D_{\underline{xy}} + D_{\underline{yx}}) & D_{\underline{xy}} &= S_{\underline{xy}} + i O_{\underline{xy}} \\ i O_{\underline{xy}} &\equiv \frac{1}{2}(D_{\underline{xy}} - D_{\underline{yx}}) \end{aligned} \quad (48)$$

and

$$W^{(symm)}_{(OAM)}(p, b) \equiv \frac{1}{2} [W(p, b) \pm (\underline{p} \rightarrow -\underline{p})], \quad (49)$$

where we have used the ‘‘OAM’’ label to indicate that the preferred direction of transverse momentum in the antisymmetric case reflects the presence of net orbital angular momentum. We can decompose W into symmetric and OAM parts for both the unpolarized distribution W_{unp} and the transversity distribution W_{trans} .

Using the (anti)symmetrized quantities in Eq. (49) we can evaluate the factors in the square

brackets of (47) as

$$\begin{aligned}
& \left[W_{unp}(p, b) D_{\underline{xy}}[+\infty, b^-] - W_{unp}(-\underline{p}, b) D_{\underline{yx}}[+\infty, b^-] \right] = \\
& \quad = 2 \left(W_{unp}^{OAM}(p, b) S_{\underline{xy}}[+\infty, b^-] + W_{unp}^{symm}(p, b) i O_{\underline{xy}}[+\infty, b^-] \right) \\
& \left[W_{trans}(p, b) D_{\underline{xy}}[+\infty, b^-] + W_{trans}(-\underline{p}, b) D_{\underline{yx}}[+\infty, b^-] \right] = \\
& \quad = 2 \left(W_{trans}^{symm}(p, b) S_{\underline{xy}}[+\infty, b^-] + W_{trans}^{OAM}(p, b) i O_{\underline{xy}}[+\infty, b^-] \right)
\end{aligned} \tag{50}$$

giving

$$\begin{aligned}
\hat{z} \cdot (\underline{J} \times \underline{k}) f_{1T}^{\perp A}(\bar{x}, k_T) &= M_A \int \frac{dp^+ d^2p db^-}{2(2\pi)^3} d^2x d^2y \frac{d^2k'}{(2\pi)^2} e^{-i(\underline{k}-\underline{k}') \cdot (\underline{x}-\underline{y})} \left\{ f_1^N(x, |\underline{k}' - x \underline{p}|) \right. \\
& \times A \left[W_{unp}^{OAM} \left(p^+, \underline{p}, b^-, \frac{\underline{x} + \underline{y}}{2} \right) S_{\underline{xy}}[+\infty, b^-] + W_{unp}^{symm} \left(p^+, \underline{p}, b^-, \frac{\underline{x} + \underline{y}}{2} \right) i O_{\underline{xy}}[+\infty, b^-] \right] \\
& + \frac{1}{m_N} \hat{z} \cdot (\underline{S} \times (\underline{k}' - x \underline{p})) f_{1T}^{\perp N}(x, |\underline{k}' - x \underline{p}|) \\
& \left. \times \left[W_{trans}^{symm} \left(p^+, \underline{p}, b^-, \frac{\underline{x} + \underline{y}}{2} \right) S_{\underline{xy}}[+\infty, b^-] + W_{trans}^{OAM} \left(p^+, \underline{p}, b^-, \frac{\underline{x} + \underline{y}}{2} \right) i O_{\underline{xy}}[+\infty, b^-] \right] \right\}.
\end{aligned} \tag{51}$$

Altogether, the symmetry arguments presented above allow us to decompose the nuclear Sivvers function $f_{1T}^{\perp A}$ into four distinct channels with the right quantum numbers to generate the T -odd asymmetry. These four channels correspond to the negative T -parity occurring in the nucleon distribution W^{OAM} , in the quark Sivvers function of the nucleon $f_{1T}^{\perp N}$, in the antisymmetric ‘‘odderon’’ rescattering iO_{xy} , or in all three simultaneously.

We now will neglect the odderon contributions in Eq. (51). The way to understand this approximation is as follows. As shown in [17], the preferred direction generated by odderon-type rescattering couples to transverse gradients of the nuclear profile function, $\nabla T(\underline{b})$. The length scale over which these gradients become important is on the order of the nuclear radius; these gradients are therefore $\mathcal{O}(A^{-1/3}) \sim \mathcal{O}(\alpha_s^2)$ suppressed (in addition to an extra power of α_s entering the lowest-order odderon amplitude corresponding to the triple-gluon exchange [52, 53, 54, 55, 56, 57, 58, 59, 17]) and are beyond the precision of the quasi-classical formula (51).

Neglecting the odderon channels in (51) we arrive at

$$\begin{aligned}
\hat{z} \cdot (\underline{J} \times \underline{k}) f_{1T}^{\perp A}(\bar{x}, k_T) &= M_A \int \frac{dp^+ d^2p db^-}{2(2\pi)^3} d^2x d^2y \frac{d^2k'}{(2\pi)^2} e^{-i(\underline{k}-\underline{k}') \cdot (\underline{x}-\underline{y})} \\
& \times \left\{ A W_{unp}^{OAM} \left(p^+, \underline{p}, b^-, \frac{\underline{x} + \underline{y}}{2} \right) f_1^N(x, |\underline{k}' - x \underline{p}|) \right. \\
& \left. + \frac{1}{m_N} \hat{z} \cdot (\underline{S} \times (\underline{k}' - x \underline{p})) W_{trans}^{symm} \left(p^+, \underline{p}, b^-, \frac{\underline{x} + \underline{y}}{2} \right) f_{1T}^{\perp N}(x, |\underline{k}' - x \underline{p}|) \right\} S_{\underline{xy}}[+\infty, b^-].
\end{aligned} \tag{52}$$

Shifting the integration variable $\underline{k}' \rightarrow \underline{k}' + x \underline{p}$ we write

$$\begin{aligned} \hat{z} \cdot (\underline{J} \times \underline{k}) f_{1T}^{\perp A}(\bar{x}, k_T) &= M_A \int \frac{dp^+ d^2 p db^-}{2(2\pi)^3} d^2 x d^2 y \frac{d^2 k'}{(2\pi)^2} e^{-i(\underline{k}-x\underline{p}-\underline{k}') \cdot (\underline{x}-\underline{y})} \\ &\times \left\{ A W_{unp}^{OAM} \left(p^+, \underline{p}, b^-, \frac{x+y}{2} \right) f_1^N(x, k'_T) \right. \\ &\left. + \frac{1}{m_N} \hat{z} \cdot (\underline{S} \times \underline{k}') W_{trans}^{symm} \left(p^+, \underline{p}, b^-, \frac{x+y}{2} \right) f_{1T}^{\perp N}(x, k'_T) \right\} S_{\underline{xy}}[+\infty, b^-]. \end{aligned} \quad (53)$$

To further simplify the obtained expression (53) we need to impose a constraint on the transverse momentum of the nucleons. Consider the nucleus in its rest frame, as shown in Fig. 6. The net OAM \vec{L} of the transversely-polarized nucleus corresponds to the rotation of

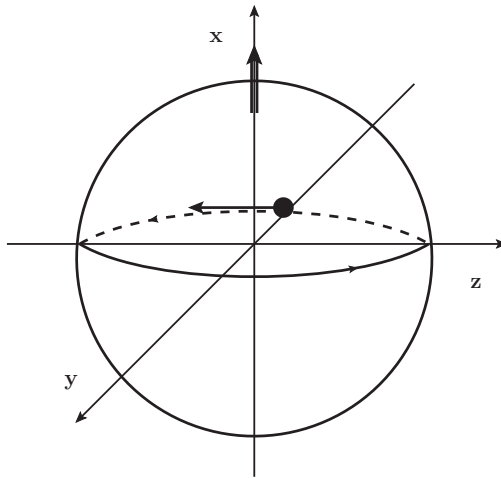


Figure 6: This figure demonstrates our axes labeling convention and helps illustrate an example discussed in the text.

the nucleus around the spin axis (the x -axis in Fig. 6). The rotational invariance around the x -axis implies that the average magnitude of the rotational transverse momentum is constant for a given distance from the x -axis and for fixed x -coordinate. (In Appendix B we show that, as a consequence of PT -symmetry, only rotational motion of the nucleons in the nucleus rest frame is allowed.)

Consider a nucleon at the point $\vec{x} = (0, -R, 0)$ in the (x, y, z) coordinate system, as illustrated by the black circle in Fig. 6. Its 3-momentum is $\vec{p}_{rest} = (0, 0, -p)$, where p denotes some typical rotational momentum of a nucleon. After a longitudinal boost along the z -axis to the infinite-momentum frame of (8) we get the large light-cone component of the momentum to be

$$p^+ = \frac{P^+}{M_A} \left(\sqrt{m_N^2 + p^2} - p \right). \quad (54)$$

The corresponding Bjorken- x is (see Eq. (9))

$$1 \geq x = \frac{-q^+}{p^+} = x_A A \frac{m_N}{\sqrt{m_N^2 + p^2} - p}, \quad (55)$$

where we have used $M_A = A m_N$. The $x \leq 1$ constraint in Eq. (55) (cf. Eq. (9)) gives

$$p \leq m_N \frac{1 - x_A^2 A^2}{2 x_A A}. \quad (56)$$

Since $x_A A$ is not a small number, in fact $x_A A = \mathcal{O}(1)$, we conclude that $p \lesssim m_N$. Therefore, the magnitude of the rotational momentum in the nuclear rest frame is bounded by $\sim m_N$ from above. The typical transverse momentum p_T in Eq. (53), being boost-invariant, is also bounded by the nucleon mass from above, $p_T \lesssim m_N$. Since we assume that k_T is perturbatively large, $k_T \gg \Lambda_{QCD} \sim m_N$, we do not consistently resum all powers of m_N/k_T . (Saturation approach resums mainly $A^{1/3}$ -enhanced power corrections, that is, powers of Q_s^2/k_T^2 , but not powers of Λ_{QCD}^2/k_T^2 .)

The bound (56) provides us with the condition on when the SIDIS process on the nucleon highlighted in Fig. 6 can take place. Violation of this bound would imply that SIDIS on that nucleon is kinematically prohibited, and consequently SIDIS may take place only on some of the other nucleons in the nucleus. While such situation where the nucleus is spinning so fast that SIDIS is only possible on a subset of its nucleons is highly unlikely in the real physical experiments, this presents a theoretical example where the Siverson function (53) would, in fact, depend on the direction of \underline{p} and, hence, of spin \underline{J} , presumably through even powers of $\underline{J} \cdot \underline{k}$. While such dependence is impossible for spin-1/2 particles such as protons [60], it has been considered for targets with different spin [61]; in our case it arises due to the classical model at hand with the value of spin J not restricted to 1/2. To avoid potential formal complications and unrealistic effects associated with large rotational momentum, below we will assume that $p_T \lesssim m_N$ such that the bound (56) is satisfied. Without such assumption, Eq. (53) would be our final result for the Siverson function in the quasi-classical approximation.

We see that we have to limit the calculation to the lowest non-trivial power of $p_T/k_T \sim m_N/k_T$ contributing to the Siverson function. Expanding Eq. (53) in the powers of \underline{p} to the lowest non-trivial order, and remembering that W^{OAM} is an odd function of \underline{p} we obtain

$$\begin{aligned} \hat{z} \cdot (\underline{J} \times \underline{k}) f_{1T}^{\perp A}(\bar{x}, k_T) &= M_A \int \frac{dp^+ d^2 p db^-}{2(2\pi)^3} d^2 x d^2 y \frac{d^2 k'}{(2\pi)^2} e^{-i(\underline{k}-\underline{k}') \cdot (\underline{x}-\underline{y})} \\ &\times \left\{ i x \underline{p} \cdot (\underline{x} - \underline{y}) A W_{unp}^{OAM} \left(p^+, \underline{p}, b^-, \frac{\underline{x} + \underline{y}}{2} \right) f_1^N(x, k'_T) \right. \\ &\left. + \frac{1}{m_N} \hat{z} \cdot (\underline{S} \times \underline{k}') W_{trans}^{symm} \left(p^+, \underline{p}, b^-, \frac{\underline{x} + \underline{y}}{2} \right) f_{1T}^{\perp N}(x, k'_T) \right\} S_{\underline{x}y}[+\infty, b^-]. \end{aligned} \quad (57)$$

Eq. (57) is our main formal result. It relates the Siverson function of a nucleus to the quark TMD and quark Siverson function in a nucleon. It shows that within the quasi-classical approximation, there are two leading channels capable of generating the Siverson function of the composite nucleus:

1. Orbital Angular Momentum (OAM) Channel: an unpolarized nucleon in a transversely polarized nucleus with a preferred direction of transverse momentum generated by the OAM of the nucleus has a quark knocked out of its symmetric f_1^N transverse momentum distribution which rescatters coherently on spectator nucleons. The multiple rescatterings bias the initial knockout process to happen near the ‘‘back’’ of the nucleus, where, due to

OAM motion of the nucleons, the outgoing quark gets an asymmetric distribution of its transverse momentum, generating STSA. (See Fig. 2 or left panel of Fig. 7 below.)

2. Transversity / Sivers Density Channel: a polarized nucleon with its preferred transverse spin direction inherited from the nucleus has a quark knocked out of its Sivers $f_{1T}^{\perp N}$ distribution which rescatters coherently on spectator nucleons. The single spin asymmetry is generated at the level of the “first” nucleon, and, unlike the OAM channel, the presence of other nucleons is not essential for this channel (see Fig. 7).

The OAM and transversity channels are depicted in Fig. 7 in terms of their space-time structure and Feynman diagrams. The diagrams resummed in arriving at Eq. (57) are the square of the graph shown in the left panel of Fig. 7 (OAM channel) and the diagram looking like the interference between the two panels in Fig. 7 (transversity channel). The difference between the two channels outlined above is in the first “knockout” interaction: the OAM channel couples to quark TMD, while the transversity channel couples to the nucleon Sivers function. At the lowest order in perturbation theory the two functions are illustrated in Fig. 8: indeed Sivers function shown in the panel B of Fig. 8 requires at least one more rescattering as compared to the quark TMD in panel A, according to the conventional wisdom [10, 11].

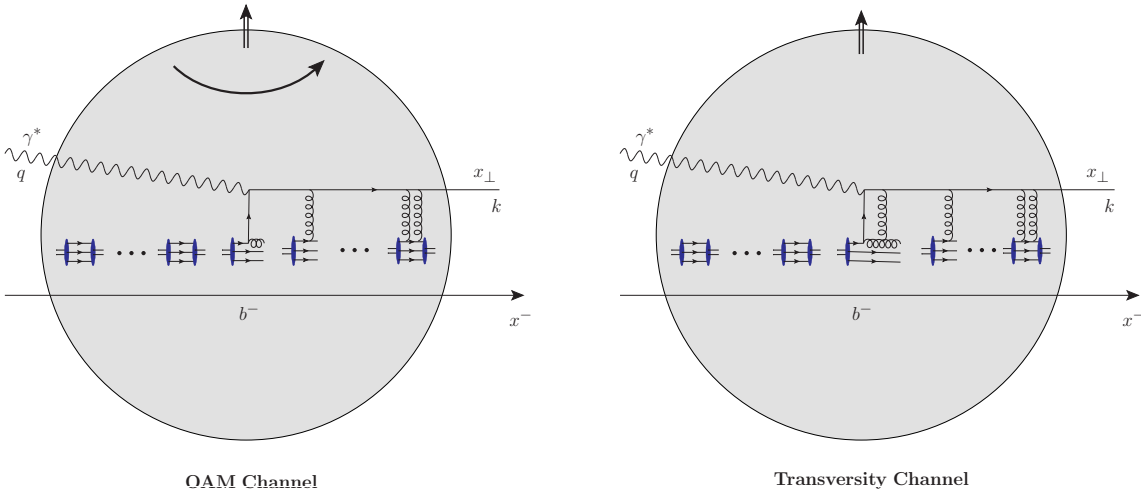


Figure 7: Side-by-side comparison of the Feynman diagrams contribution to the OAM and Sivers density channels in the quasi-classical approximation (in the rest frame of the nucleus).

Note that, in the OAM channel, the unpolarized quark distribution f_1^N enters parametrically at $\mathcal{O}(\alpha_s A^{1/3})$ if calculated at the lowest-order in the perturbation theory (see panel A in Fig. 8), which is $\mathcal{O}(\alpha_s^{-1})$ in the saturation power counting (where $\alpha_s^2 A^{1/3} \sim 1$). In the transversity channel, the nucleonic Sivers function $f_{1T}^{\perp N}$ enters at $\mathcal{O}(\alpha_s^2 A^{1/3}) = \mathcal{O}(1)$ at the lowest order in perturbation theory, because it requires an extra $\mathcal{O}(\alpha_s)$ gluon to be exchanged with the same nucleon to obtain the necessary lensing effect [10] (see panel B in Fig. 8). The transversity channel is therefore $\mathcal{O}(1)$ in the saturation power counting and is subleading by $\mathcal{O}(\alpha_s)$ to the OAM channel in this sense.⁶ Indeed the non-trivial transverse motion of nucleons due to OAM

⁶We would like to point out that the coupling constant α_s in f_1^N runs with some non-perturbative momentum scale, and is large, $\alpha_s = \alpha_s(\sim \Lambda_{QCD}^2)$; however, a simple application of the BLM [51] prescription to the

should be present for the OAM channel to be non-zero: this channel is leading only if there is an OAM. In our estimate here we have assumed that the net spin of our “nucleons” scales linearly with the atomic number, $S \sim A$; perhaps a more realistic (both for protons and nuclei) slower growth of S with A would introduce extra A -suppression for the transversity channel.

Despite the transversity channel being subleading, it is more dominant than the $\mathcal{O}(A^{-1/3}) \sim \mathcal{O}(\alpha_s^2)$ corrections we neglected when arriving at the quasi-classical formula (57) (again, for $S \sim A$). Order α_s^1 quantum corrections to the OAM channel also enter at the same order as the nucleonic Sivers function and are also within the precision of the formalism.

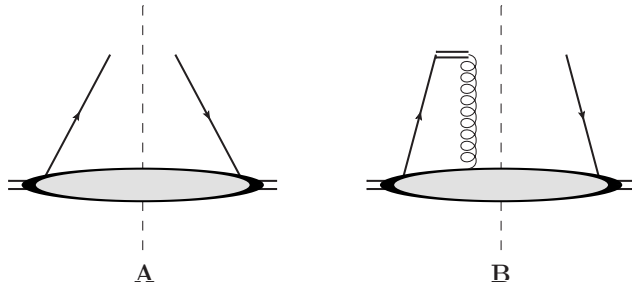


Figure 8: Lowest-order diagrams for the quark TMD f_1 (panel A) and the Sivers function f_{1T}^\perp (panel B). Vertical dashed line denotes the final state cut, while the double horizontal line in panel B denotes the Wilson line.

An essential role is played by the rescattering factor $S_{\underline{xy}}[+\infty, b^-]$ in the OAM channel. The Wigner function due to orbital motion of nucleons around the axis of the transverse spin is an odd function of the longitudinal coordinate b_z in the rest frame of the nucleus,

$$W_{unp}^{OAM}(p, \underline{b}, b_z) = -W_{unp}^{OAM}(p, \underline{b}, -b_z), \quad (58)$$

which follows simply from the fact that in the left panel of Fig. 7 we have as many nucleons moving outside the page to the left of the nuclear center as there are nucleons moving into the page to the right of the nuclear center. In Appendix B we show how the result (58) can be obtained by requiring that our “nucleus” is PT -symmetric. The b^- -integral of the first term in the curly brackets of Eq. (57) would have been zero, if it was not for the b^- -dependent factor of $S_{\underline{xy}}[+\infty, b^-]$. This multiple-rescattering factor approaches 1 for b^- values near the “back” of the nucleus (right end of the nucleus in Fig. 7) and is a monotonically decreasing function of b^- . Due to this factor, different b^- regions contribute differently to the integral, making it non-zero. The region near the “back” of the nucleus dominates, which has a physical interpretation that it is easier for the quark to escape the nucleus if it is produced near the edge. Hence we arrive at the interpretation of the SIDIS in the OAM channel outlined in the Introduction: the quarks are produced predominantly toward the “back” of the nucleus, where the nucleons rotate preferentially into the page (see left panel of Fig. 7 or Fig. 2). Therefore, the quark has more transverse momentum into the page than out of the page, which leads to STSA for the produced quarks.

calculation of [21] can show that in $f_{1T}^{\perp N}(x, k_T)$ the two powers of the coupling run as $\alpha_s(k_T^2) \alpha_s(\sim \Lambda_{QCD}^2)$. While one of the couplings is also non-perturbatively large, the other one is perturbatively small for $k_T \gg \Lambda_{QCD}$, indicating suppression.

To complete Eq. (57) we need to construct an expression for the nuclear spin $\vec{J} = \vec{L} + \vec{S}$. The OAM of the nucleons in the nucleus from Fig. 6 in the nuclear rest frame is

$$\vec{L} = A \int \frac{d^3p d^3b}{2(2\pi)^3} W_{unp}(\vec{p}, \vec{b}) \vec{b} \times \vec{p} = A \int \frac{d^3p d^3b}{2(2\pi)^3} W_{unp}(\vec{p}, \vec{b}) \hat{x} (b_y p_z - b_z p_y), \quad (59)$$

where $d^3p = dp_x dp_y dp_z$, $d^3b = db_x db_y db_z$, and $W_{unp}(\vec{p}, \vec{b})$ is the Wigner distribution in the rest frame of the nucleus expressed in terms of 3-vectors $\vec{p} = (p_x, p_y, p_z)$ and $\vec{b} = (b_x, b_y, b_z)$.

To boost this into the infinite momentum frame of (8) we define the Pauli-Lubanski vector of the nuclear spin

$$W_\mu = -\frac{1}{2} \epsilon_{\mu\nu\rho\sigma} J^{\nu\rho} P^\sigma, \quad (60)$$

where $J_{\mu\nu} = L_{\mu\nu} + S_{\mu\nu}$ with $L_{\mu\nu}$ and $S_{\mu\nu}$ the expectation values of the OAM and spin generators of the Lorentz group in the nuclear state. The OAM generator is

$$\hat{L}_{\mu\nu} = \hat{x}_\mu \hat{p}_\nu - \hat{x}_\nu \hat{p}_\mu \quad (61)$$

as usual, with the hat denoting operators. The nuclear OAM four-vector is then defined by

$$L_\mu = -\frac{1}{2} \epsilon_{\mu\nu\rho\sigma} L^{\nu\rho} \frac{P^\sigma}{M_A}. \quad (62)$$

Note that \hat{p}_μ in Eq. (61) are the momentum operators of the nucleons, while P^σ in Eqs. (60) and (62) is the net momentum of the whole nucleus. In the rest frame of the nucleus Eq. (62) gives $L_x = L_{yz}$ as expected (for $\epsilon_{0123} = +1$). The nuclear OAM four-vector can then be written as

$$L_\mu = -\frac{1}{2} \epsilon_{\mu\nu\rho\sigma} \frac{P^\sigma}{M_A} A \int \frac{dp^+ d^2p db^- d^2b}{2(2\pi)^3} W_{unp}(p, b) (b^\nu p^\rho - b^\rho p^\nu) \quad (63)$$

in the infinite momentum frame of the nucleus.

Since boosts preserve transverse components of four-vectors, the boost along the \hat{z} -axis of the nucleus in Fig. 6 would preserve its OAM three-vector \vec{L} . Hence Eq. (59) gives us the transverse components of OAM in the infinite momentum frame as well. We thus write

$$\vec{J} = \hat{x} \left[S + A \int \frac{d^3p d^3b}{2(2\pi)^3} W_{unp}(\vec{p}, \vec{b}) \hat{x} (b_y p_z - b_z p_y) \right], \quad (64)$$

where the integration over p and b needs to be carried out in the nucleus rest frame.

Combining Eqs. (57) with (64) allows one to extract the Sivers function $f_{1T}^{\perp A}$ of the nucleus.

3.3 Comparison of the OAM and Transversity Channels in the SIDIS Sivers Function

We will now illustrate the properties of the Sivers function (57) by studying a specific simplified example. Consider the model of the nucleus as a non-relativistic rigid rotator, with the

rotational momentum in its rest frame being much smaller than the nucleon mass, $p_T \ll m_N$. The corresponding classical Wigner distribution is (cf. Eq. (31))

$$W_{unp}(p, b) \approx \frac{2(2\pi)^3}{A} \rho(\underline{b}, b^-) \delta^2 \left(\underline{p} - \hat{y} p_{max}(b_x) \frac{b^-}{R^-(b_x)} \right) \delta \left(p^+ - \frac{P^+}{A} \right), \quad (65)$$

where $2R^-(b_x)$ is the extent of the nucleus in the b^- -direction at $\underline{b} = (b_x, 0)$ (with $R^-(b_x) = \sqrt{R^2 - b_x^2} M_A/P^+$), and $p_{max}(b_x) = p_{max} \sqrt{R^2 - b_x^2}/R$ is the maximum value of the rotational momentum at a given b_x . In writing down the distribution (65) we have neglected possible longitudinal rotational motion of the nucleons, which is justified in the $p_T \ll m_N$ limit. We also assume that a fraction β of the nucleons in the nucleus are polarized in the $+\hat{x}$ -direction, such that their net spin is $S = \beta A/2$ and (see Eq. (44))

$$W_{trans}(p, b) = \beta W_{unp}(p, b). \quad (66)$$

Substituting Eqs. (65) and (66) into Eq. (57) and integrating over p^+ and \underline{p} yields

$$J k_y f_{1T}^{\perp A}(\bar{x}, k_T) = M_A \int db^- d^2x d^2y \rho \left(\frac{\underline{x} + \underline{y}}{2}, b^- \right) \frac{d^2k'}{(2\pi)^2} e^{-i(\underline{k} - \underline{k}') \cdot (\underline{x} - \underline{y})} \left\{ i \bar{x} \right. \\ \left. \times p_{max} \left(\frac{(\underline{x} + \underline{y})_x}{2} \right) \frac{b^-}{R^-((\frac{\underline{x} + \underline{y}}{2})_x)} (\underline{x} - \underline{y})_y f_1^N(\bar{x}, k'_T) + \frac{\beta}{2m_N} k'_y f_{1T}^{\perp N}(\bar{x}, k'_T) \right\} S_{\underline{x}\underline{y}}[+\infty, b^-], \quad (67)$$

where we also replaced \vec{J} by $\hat{x} J$ and \vec{S} by $\hat{x} (\beta A/2)$.

To further simplify Eq. (67) we need to make specific assumptions about the form of f_1^N and $f_{1T}^{\perp N}$. Inspired by the lowest-order expressions for both quantities [62, 48, 21] we write

$$f_1^N(x, k_T) = \frac{\alpha_s C_1}{k_T^2}, \quad f_{1T}^{\perp N}(x, k_T) = \frac{\alpha_s^2 m_N^2 C_2}{k_T^4} \ln \frac{k_T^2}{\Lambda^2}, \quad (68)$$

where C_1 and C_2 are some x -dependent functions and Λ is an infrared cutoff. Inserting Eq. (68) into Eq. (67) and integrating over k'_T yields

$$J k_y f_{1T}^{\perp A}(\bar{x}, k_T) = \frac{\alpha_s M_A}{2\pi} \int db^- d^2x d^2y \rho \left(\frac{\underline{x} + \underline{y}}{2}, b^- \right) e^{-i\underline{k} \cdot (\underline{x} - \underline{y})} (\underline{x} - \underline{y})_y \left\{ i \bar{x} \right. \\ \left. \times p_{max} \left(\frac{(\underline{x} + \underline{y})_x}{2} \right) \frac{b^- C_1}{R^-((\frac{\underline{x} + \underline{y}}{2})_x)} \ln \frac{1}{|\underline{x} - \underline{y}| \Lambda} + \frac{i \alpha_s m_N \beta C_2}{4} \ln^2 \frac{1}{|\underline{x} - \underline{y}| \Lambda} \right\} S_{\underline{x}\underline{y}}[+\infty, b^-]. \quad (69)$$

In the classical MV/GM approximation the (symmetric part of the) dipole scattering matrix is [25]

$$S_{\underline{x}\underline{y}}[+\infty, b^-] = \exp \left[-\frac{1}{4} |\underline{x} - \underline{y}|^2 Q_s^2 \left(\frac{\underline{x} + \underline{y}}{2} \right) \left(\frac{R^-(\underline{b}) - b^-}{2R^-(\underline{b})} \right) \ln \frac{1}{|\underline{x} - \underline{y}| \Lambda} \right], \quad (70)$$

where $R^-(\underline{b}) = \sqrt{R^2 - \underline{b}^2} M_A/P^+$ and the quark saturation scale is

$$Q_s^2(\underline{b}) = 4\pi \alpha_s^2 \frac{C_F}{N_c} T(\underline{b}) \quad (71)$$

with the nuclear profile function

$$T(\underline{b}) = \int db^- \rho(\underline{b}, b^-). \quad (72)$$

As usual N_c is the number of colors and $C_F = (N_c^2 - 1)/2N_c$ is the Casimir operator of $SU(N_c)$ in the fundamental representation. In arriving at Eq. (70) we assumed that the nuclear density is constant within the nucleus, such that

$$\rho(\underline{b}, b^-) = \frac{\theta(R^-(\underline{b}) - |b^-|)}{2R^-(\underline{b})} T(\underline{b}). \quad (73)$$

Employing Eq. (70) along with Eqs. (73) and (71), and neglecting all logarithms $\ln(1/|\underline{x} - \underline{y}|/\Lambda)$ (which is justified as long as k_T is not too much larger than Q_s [63]) we can integrate Eq. (69) over b^- and $\underline{x} - \underline{y}$ obtaining

$$f_{1T}^{\perp A}(\bar{x}, k_T) = \frac{M_A N_c}{4\pi \alpha_s J C_F} \frac{1}{k_T^2} \int d^2b \left\{ 4\bar{x} p_{max}(\underline{b}) C_1 \left[e^{-k_T^2/Q_s^2(\underline{b})} + 2 \frac{k_T^2}{Q_s^2(\underline{b})} Ei \left(-\frac{k_T^2}{Q_s^2(\underline{b})} \right) \right] + \alpha_s \beta m_N C_2 e^{-k_T^2/Q_s^2(\underline{b})} \right\}, \quad (74)$$

where now $\underline{b} = (\underline{x} + \underline{y})/2$ and $p_{max}(\underline{b}) = p_{max} \sqrt{R^2 - \underline{b}^2}/R$. The \underline{b} -integral appears to be rather hard to perform for a realistic spherical nucleus: we leave expression (74) in its present form.

To obtain a final expression for the Siverson function we need to determine the spin of the nucleus J . For a rigid rotator spinning around the \hat{x} -axis with the maximum nucleon momentum p_{max} we readily get

$$L = \frac{4}{5} A p_{max} R \quad (75)$$

in the nuclear rest frame. Using this in Eq. (64) along with $S = \beta A/2$ we obtain

$$J = \beta \frac{A}{2} + \frac{4}{5} A p_{max} R. \quad (76)$$

Inserting Eq. (76) into Eq. (74) gives

$$f_{1T}^{\perp A}(\bar{x}, k_T) = \frac{m_N N_c}{2\pi \alpha_s C_F} \frac{1}{\beta + \frac{8}{5} p_{max} R} \frac{1}{k_T^2} \times \int d^2b \left\{ 4\bar{x} p_{max}(\underline{b}) C_1 \left[e^{-k_T^2/Q_s^2(\underline{b})} + 2 \frac{k_T^2}{Q_s^2(\underline{b})} Ei \left(-\frac{k_T^2}{Q_s^2(\underline{b})} \right) \right] + \alpha_s \beta m_N C_2 e^{-k_T^2/Q_s^2(\underline{b})} \right\}. \quad (77)$$

Eq. (77) is our final expression for the Siverson function of a nucleus in the quasi-classical approximation with the rigid rotator model for the nucleus and k_T not too much larger than Q_s . Analyzing this expression we see that the OAM term (the first term in the curly brackets) does change sign as a function of k_T , while the Siverson density term (the second term in the curly brackets of Eq. (77)) is positive-definite. Still the first term in the curly brackets is positive for most of the k_T domain, in agreement with the qualitative argument in the Introduction corresponding to quarks being produced preferentially into the page in Fig. 2.

To study the $k_T \gg Q_s$ case we have to return to Eq. (69): this time we do not neglect the logarithms. Large k_T limit implies that $|\underline{x} - \underline{y}|$ is small, and we need to expand the exponential in Eq. (70) to the lowest non-trivial (contributing) order in each term in Eq. (69). For the Siverson density term this corresponds to replacing the exponent by 1. The remaining evaluation is easier to carry out in Eq. (67), which yields an intuitively clear formula

$$J f_{1T}^{\perp A}(\bar{x}, k_T) \Big|_{\text{transversivity channel, } k_T \gg Q_s} = A S f_{1T}^{\perp N}(\bar{x}, k_T). \quad (78)$$

In the first term in the curly brackets of Eq. (69) we need to expand the exponential in $S_{\underline{x}\underline{y}}[+\infty, b^-]$ one step further, obtaining after some straightforward algebra for the whole SIDIS Siverson function

$$\begin{aligned} f_{1T}^{\perp A}(\bar{x}, k_T) \Big|_{k_T \gg Q_s} &= \frac{S}{J} \left[-\frac{4\alpha_s m_N \bar{x} C_1}{3\beta k_T^6} \ln \frac{k_T^2}{\Lambda^2} \int d^2b T(\underline{b}) p_{max}(\underline{b}) Q_s^2(\underline{b}) + A f_{1T}^{\perp N}(\bar{x}, k_T) \right] \\ &= \frac{\beta}{\beta + \frac{8}{5} p_{max} R} \left[-\frac{4\alpha_s m_N \bar{x} C_1}{3\beta k_T^6} \ln \frac{k_T^2}{\Lambda^2} \int d^2b T(\underline{b}) p_{max}(\underline{b}) Q_s^2(\underline{b}) + \frac{A \alpha_s^2 m_N^2 C_2}{k_T^4} \ln \frac{k_T^2}{\Lambda^2} \right]. \quad (79) \end{aligned}$$

Since

$$\int d^2b T(\underline{b}) = A \quad (80)$$

we see that the OAM channel contribution in Eq. (79) (the first term) is proportional to $A \alpha_s m_N p_T Q_s^2/k_T^6$, while the transversivity channel contribution (the second term) scales as $A \alpha_s^2 m_N^2/k_T^4$. (Note that $x = \mathcal{O}(1)$, such that powers of x do not generate suppression.) Assuming that $p_T \approx m_N$ (see the discussion following Eq. (56)) we observe that the ratio of the OAM to transversivity channel contributions is $\sim Q_s^2/(\alpha_s k_T^2)$. (Note that for $p_T \approx m_N$ the prefactor of Eq. (79) gives a factor $\sim 1/(m_N R) \approx A^{-1/3}$ multiplying both terms, but not affecting their ratio.) We conclude that the OAM channel dominates for

$$k_T < \frac{Q_s}{\sqrt{\alpha_s}}, \quad (81)$$

that is both inside the saturation region, and in a sector of phase space outside that region. For $k_T > Q_s/\sqrt{\alpha_s}$ the transversivity channel dominates, mapping onto the expected perturbative QCD result (78).

While the main aim of this calculation is to model a nucleon at high energies, a few comments are in order about the application of this rigid rotator toy model to a realistic nucleus. Certainly a classical rigid rotator is a poor model for a real nucleus; a better approach would be to use our general result (57) with the Wigner distribution $W(p, b)$ given by the realistic single-particle wave functions taken from nuclear structure calculations. In such realistic cases, the total angular momentum J of the nucleus is typically small, and the fraction β that comes from the nucleons' spins is also small due to nucleon spin pairing. If one were to approximate a real nucleus with this rigid rotator toy model, appropriately small J and β would need to be used in (77) and (79). The smallness of the total OAM J does not affect the Siverson function $f_{1T}^{\perp A}$ because the magnitude is contained in the prefactor $\hat{z} \cdot (\underline{J} \times \underline{k})$ and cancels in the S/J ratio. The smallness of the spin contribution $\beta \sim \mathcal{O}(1/A)$, however, would suppress the transversivity channel and ensure the dominance of the OAM term. But regardless of its applicability to a real nucleus, the rigid rotator toy model illustrates the ability of this formalism to capture the interplay of spin and angular momentum in a dense system at high energy.

4 Drell-Yan Process

We now wish to perform a similar analysis for the Drell-Yan process $\bar{q} + A^\dagger \rightarrow \gamma^* + X \rightarrow \ell^+ \ell^- + X$, where the antiquark from the unpolarized hadron scatters on the transversely polarized hadron/nucleus, producing a space-like photon which later decays into a di-lepton pair. The annihilation sub-process $\bar{q} + q^\dagger \rightarrow \gamma^* + X$ is related to the SIDIS process by time reversal, which leads to the famous prediction [11] that the Sivers functions entering observables in the two processes should have equal magnitudes and opposite signs.

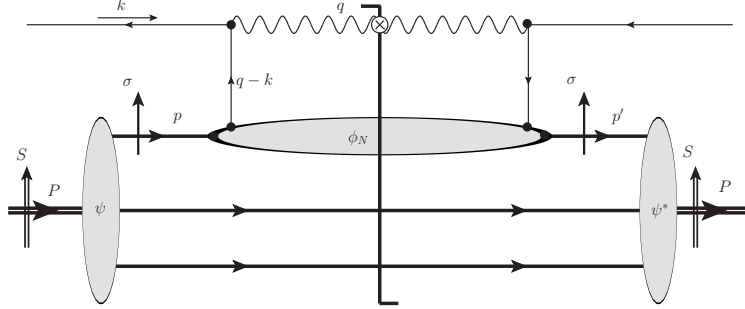


Figure 9: Lowest-order DY process in the usual α_s power-counting. An antiquark from a projectile hadron annihilates with a quark from a nucleon in the target nucleus, producing a highly virtual photon which then decays into a di-lepton pair (not shown).

The lowest-order Drell-Yan annihilation process is shown in Fig. 9, without including initial-state rescattering of the antiquark on nuclear spectators. Labeling the momenta as in Fig. 9 and following along the same lines as for SIDIS, we can write the kinematics in the $\bar{q} + A^\dagger$ center-of-mass frame as

$$\begin{aligned}
 P^\mu &= (P^+, M_A^2/P^+, \underline{0}) \\
 p^\mu &= (p^+, (p_T^2 + m_N^2)/p^+, \underline{p}) \\
 k^\mu &= (\frac{m_q^2}{Q^2} q^+, k^- \approx q^-, \underline{0}) \\
 q^\mu &= (q^+, q^- \approx Q^2/q^+, \underline{q}),
 \end{aligned} \tag{82}$$

where

$$\begin{aligned}
 \hat{s} &\equiv (p + k)^2 \approx p^+ q^- \\
 x &\equiv \frac{Q^2}{2p \cdot q} \approx \frac{Q^2}{\hat{s}} \approx \frac{q^+}{p^+}.
 \end{aligned} \tag{83}$$

As with SIDIS, we are working in the kinematic limit $s_A = (P + k)^2 \gg \hat{s}, Q^2 \gg \perp^2$, with $\alpha \equiv p^+/P^+ \approx s_A/\hat{s} \sim \mathcal{O}(1/A)$. Again, we can compare the coherence lengths $\ell_k^- \sim 1/k^+$ of the antiquark and $\ell_\gamma^- \sim 1/q^+$ of

$$\begin{aligned}
 \frac{\ell_k^-}{L^-} &\sim \frac{1}{x} \left(\frac{Q^2}{m_q^2} \right) \frac{1}{\alpha M_A R} \sim \mathcal{O} \left(\frac{Q^2}{m_q^2} A^{-1/3} \right) \gg 1 \\
 \frac{\ell_\gamma^-}{L^-} &\sim \frac{1}{x} \frac{1}{\alpha M_A R} \sim \mathcal{O}(A^{-1/3}) \ll 1.
 \end{aligned} \tag{84}$$

Analogous to SIDIS, this shows that the coherence length of the incoming antiquark is large; in fact it would be infinite if we dropped the quark mass m_q as we have elsewhere in the calculation. We conclude that the long-lived antiquark is able to rescatter off of many nucleons before it finally annihilates a quark. The annihilation occurs locally, as indicated by the short coherence length of the virtual photon, and thereafter the produced photon / dilepton system does not rescatter hadronically. This again motivates the resummation of these initial state rescatterings into a Wilson line dipole trace.

4.1 Quasi-Classical Sivers Function in DY

The entire Drell-Yan (DY) process in the quasi-classical approximation is shown in Fig. 10 at the level of the scattering amplitude: the incoming antiquark coherently scatters on the nucleon in the transversely polarized nucleons, until the last interaction in which the virtual photon is produced, which later generated the di-lepton pair.⁷

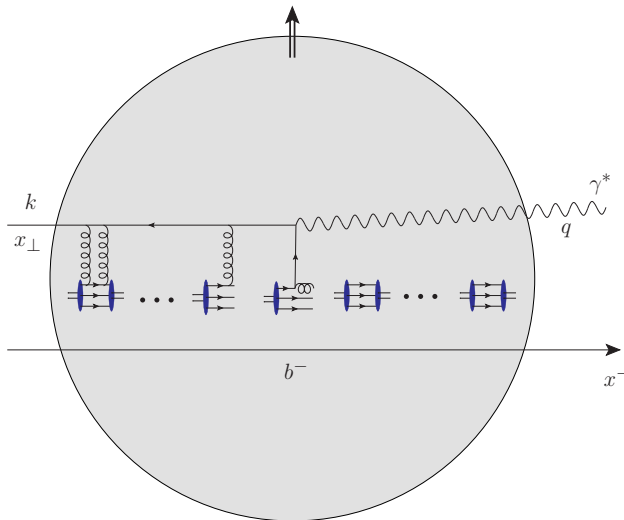


Figure 10: Space-time structure of the quasi-classical DY process in the rest frame of the nucleus, overlaid with one of the corresponding Feynman diagrams. The shaded circle is the transversely polarized nucleus, with the vertical double arrow denoting the spin direction.

By analogy with Eq. (36) in SIDIS we write the following relation for the quark correlators in DY,

$$\begin{aligned} \text{Tr}[\Phi_A(\bar{x}, \underline{q}; P, J)\gamma^+] &= A \int \frac{dp^+ d^2p db^-}{2(2\pi)^3} \int \frac{d^2k' d^2x d^2y}{(2\pi)^2} e^{ik' \cdot (\underline{x} - \underline{y})} \sum_{\sigma} W_N^{\sigma} \left(p, b^-, \frac{\underline{x} + \underline{y}}{2} \right) \\ &\times \text{Tr}[\phi_N(x, \underline{q} - \underline{k}' - x \underline{p}); p, \sigma)\gamma^+] D_{\underline{y}\underline{x}}[b^-, -\infty], \end{aligned} \quad (85)$$

where

$$D_{\underline{y}\underline{x}}[b^-, -\infty] = \left\langle \frac{1}{N_c} \text{Tr} \left[V_{\underline{y}}[b^-, -\infty] V_{\underline{x}}^{\dagger}[b^-, -\infty] \right] \right\rangle \quad (86)$$

⁷Just like for SIDIS, in small- x physics the DY process is dominated by the $\bar{q} + A \rightarrow \gamma^* + \bar{q} + A$ scattering [64], which is $\mathcal{O}(\alpha_s)$ -subleading compared to the diagram in Fig. 10: since in our calculation $x = \mathcal{O}(1)$, we will neglect the $\bar{q} + A \rightarrow \gamma^* + \bar{q} + A$ process here as an $\mathcal{O}(\alpha_s)$ correction.

and the quark correlators are defined by equations similar to (37) and (38), but now using a different gauge link (5):

$$\Phi_{ij}^A(\bar{x}, \underline{k}; P, J) \equiv \int \frac{dx^- d^2x_\perp}{2(2\pi)^3} e^{i(\frac{1}{2}\bar{x}P^+ x^- - \underline{x}\cdot\underline{k})} \langle A; P, J | \bar{\psi}_j(0) \mathcal{U}^{DY} \psi_i(x^+ = 0, x^-, \underline{x}) | A; P, J \rangle, \quad (87)$$

$$\phi_{ij}^N(x, \underline{k}; p, \sigma) \equiv \int \frac{dx^- d^2x_\perp}{2(2\pi)^3} e^{i(\frac{1}{2}x p^+ x^- - \underline{x}\cdot\underline{k})} \langle N; p, \sigma | \bar{\psi}_j(0) \mathcal{U}^{DY} \psi_i(x^+ = 0, x^-, \underline{x}) | N; p, \sigma \rangle. \quad (88)$$

Here $\bar{x} = A q^+ / P^+$. Eq. (85) is illustrated in Fig. 11. The main difference compared to Eq. (36) is that now $\underline{k} = 0$ and $\underline{q} \neq 0$.

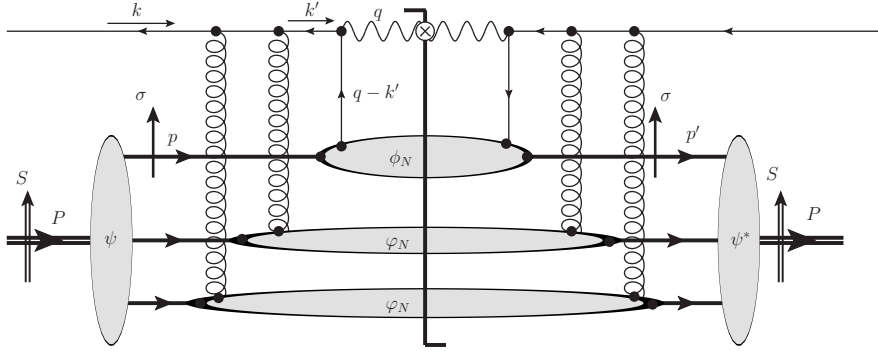


Figure 11: Decomposition of the nuclear quark distribution Φ_A probed by the DY process into mean-field wave functions ψ, ψ^* of nucleons and the quark and gluon distributions ϕ_N and φ_N of the nucleons.

Projecting out the DY Siverts function of the nucleus $f_{1T}^{\perp A}$ using (41) gives

$$\hat{z} \cdot (\underline{J} \times \underline{q}) f_{1T}^{\perp A}(\bar{x}, q_T) = \frac{M_A A}{4} \int \frac{dp^+ d^2p db^-}{2(2\pi)^3} \int \frac{d^2k' d^2x d^2y}{(2\pi)^2} e^{ik' \cdot (\underline{x} - \underline{y})} \sum_{\sigma} W_N^{\sigma} \left(p, b^-, \frac{\underline{x} + \underline{y}}{2} \right) \times \text{Tr}[\phi_N(x, \underline{q} - \underline{k}' - x \underline{p}); p, \sigma) \gamma^+] D_{\underline{y}\underline{x}}[b^-, -\infty] - (\underline{q} \rightarrow -\underline{q}). \quad (89)$$

With the help of Eq. (40b) we write

$$\hat{z} \cdot (\underline{J} \times \underline{q}) f_{1T}^{\perp A}(\bar{x}, q_T) = \frac{M_A A}{2} \int \frac{dp^+ d^2p db^-}{2(2\pi)^3} \int \frac{d^2k' d^2x d^2y}{(2\pi)^2} e^{ik' \cdot (\underline{x} - \underline{y})} \sum_{\sigma} W_N^{\sigma} \left(p, b^-, \frac{\underline{x} + \underline{y}}{2} \right) \times \left[f_1^N(x, |\underline{q} - \underline{k}' - x \underline{p}|_T) + \frac{1}{m_N} \hat{z} \cdot (\underline{\sigma} \times (\underline{q} - \underline{k}' - x \underline{p})) f_{1T}^{\perp N}(x, |\underline{q} - \underline{k}' - x \underline{p}|_T) \right] \times D_{\underline{y}\underline{x}}[b^-, -\infty] - (\underline{q} \rightarrow -\underline{q}). \quad (90)$$

Performing the spin sums (44) gives

$$\begin{aligned}
\hat{z} \cdot (\underline{J} \times \underline{q}) f_{1T}^{\perp A}(\bar{x}, q_T) &= \frac{M_A}{2} \int \frac{dp^+ d^2 p db^-}{2(2\pi)^3} \int \frac{d^2 k' d^2 x d^2 y}{(2\pi)^2} e^{ik' \cdot (\underline{x} - \underline{y})} \left[A W_{unp} \left(p, b^-, \frac{\underline{x} + \underline{y}}{2} \right) \right. \\
&\times f_1^N(x, |\underline{q} - \underline{k}' - x \underline{p}|_T) + W_{trans} \left(p, b^-, \frac{\underline{x} + \underline{y}}{2} \right) \frac{1}{m_N} \hat{z} \cdot (\underline{S} \times (\underline{q} - \underline{k}' - x \underline{p})) \\
&\left. \times f_{1T}^{\perp N}(x, |\underline{q} - \underline{k}' - x \underline{p}|_T) \right] D_{\underline{y}\underline{x}}[b^-, -\infty] - (\underline{q} \rightarrow -\underline{q}). \tag{91}
\end{aligned}$$

In the terms being subtracted in Eq. (91) with $(\underline{q} \rightarrow -\underline{q})$, we can also reverse the dummy integration variables $\underline{k}' \rightarrow -\underline{k}'$, $\underline{p} \rightarrow -\underline{p}$, and $\underline{x} \leftrightarrow \underline{y}$. This leaves the Fourier factor and the distributions f_1^N , $f_{1T}^{\perp N}$ invariant, giving

$$\begin{aligned}
\hat{z} \cdot (\underline{J} \times \underline{q}) f_{1T}^{\perp A}(\bar{x}, q_T) &= \frac{M_A}{2} \int \frac{dp^+ d^2 p db^-}{2(2\pi)^3} \int \frac{d^2 k' d^2 x d^2 y}{(2\pi)^2} e^{ik' \cdot (\underline{x} - \underline{y})} \left\{ f_1^N(x, |\underline{q} - \underline{k}' - x \underline{p}|_T) \right. \\
&\times A \left[W_{unp} \left(p^+, \underline{p}, b^-, \frac{\underline{x} + \underline{y}}{2} \right) D_{\underline{y}\underline{x}}[b^-, -\infty] - W_{unp} \left(p^+, -\underline{p}, b^-, \frac{\underline{x} + \underline{y}}{2} \right) D_{\underline{x}\underline{y}}[b^-, -\infty] \right] \\
&+ \frac{1}{m_N} \hat{z} \cdot (\underline{S} \times (\underline{q} - \underline{k}' - x \underline{p})) f_{1T}^{\perp N}(x, |\underline{q} - \underline{k}' - x \underline{p}|_T) \\
&\left. \times \left[W_{trans} \left(p^+, \underline{p}, b^-, \frac{\underline{x} + \underline{y}}{2} \right) D_{\underline{y}\underline{x}}[b^-, -\infty] + W_{trans} \left(p^+, -\underline{p}, b^-, \frac{\underline{x} + \underline{y}}{2} \right) D_{\underline{x}\underline{y}}[b^-, -\infty] \right] \right\}. \tag{92}
\end{aligned}$$

We recognize the factors in brackets from the SIDIS case (50), rewriting (92) as

$$\begin{aligned}
\hat{z} \cdot (\underline{J} \times \underline{q}) f_{1T}^{\perp A}(\bar{x}, q_T) &= M_A \int \frac{dp^+ d^2 p db^-}{2(2\pi)^3} \int \frac{d^2 k' d^2 x d^2 y}{(2\pi)^2} e^{ik' \cdot (\underline{x} - \underline{y})} \left\{ f_1^N(x, |\underline{q} - \underline{k}' - x \underline{p}|_T) \right. \\
&\times A \left[W_{unp}^{OAM} \left(p^+, \underline{p}, b^-, \frac{\underline{x} + \underline{y}}{2} \right) S_{\underline{y}\underline{x}}[b^-, -\infty] + W_{unp}^{symm} \left(p^+, -\underline{p}, b^-, \frac{\underline{x} + \underline{y}}{2} \right) i O_{\underline{y}\underline{x}}[b^-, -\infty] \right] \\
&+ \frac{1}{m_N} \hat{z} \cdot (\underline{S} \times (\underline{q} - \underline{k}' - x \underline{p})) f_{1T}^{\perp N}(x, |\underline{q} - \underline{k}' - x \underline{p}|_T) \\
&\left. \times \left[W_{trans}^{symm} \left(p^+, \underline{p}, b^-, \frac{\underline{x} + \underline{y}}{2} \right) S_{\underline{y}\underline{x}}[b^-, -\infty] + W_{trans}^{OAM} \left(p^+, -\underline{p}, b^-, \frac{\underline{x} + \underline{y}}{2} \right) i O_{\underline{y}\underline{x}}[b^-, -\infty] \right] \right\}. \tag{93}
\end{aligned}$$

As before, we drop contributions from the odderon $iO_{\underline{y}\underline{x}}$ as being outside the precision of the quasi-classical formula (85) to get

$$\begin{aligned}
\hat{z} \cdot (\underline{J} \times \underline{q}) f_{1T}^{\perp A}(\bar{x}, q_T) &= M_A \int \frac{dp^+ d^2 p db^-}{2(2\pi)^3} \int \frac{d^2 k' d^2 x d^2 y}{(2\pi)^2} e^{ik' \cdot (\underline{x} - \underline{y})} \\
&\times \left\{ A W_{unp}^{OAM} \left(p^+, \underline{p}, b^-, \frac{\underline{x} + \underline{y}}{2} \right) f_1^N(x, |\underline{q} - \underline{k}' - x \underline{p}|_T) \right. \\
&\left. + \frac{1}{m_N} \hat{z} \cdot (\underline{S} \times (\underline{q} - \underline{k}' - x \underline{p})) W_{trans}^{symm} \left(p^+, \underline{p}, b^-, \frac{\underline{x} + \underline{y}}{2} \right) f_{1T}^{\perp N}(x, |\underline{q} - \underline{k}' - x \underline{p}|_T) \right\} S_{\underline{y}\underline{x}}[b^-, -\infty]. \tag{94}
\end{aligned}$$

Since the rotational momentum of the nucleons p_T is assumed to be small, we have to expand in it to the lowest non-trivial order. Shifting the integration variable $\underline{k}' \rightarrow \underline{k}' + \underline{q} - x \underline{p}$

in Eq. (94) and expanding the exponential to the lowest non-trivial order in p_T we obtain (cf. Eq. (57))

$$\begin{aligned} \hat{z} \cdot (\underline{J} \times \underline{q}) f_{1T}^{\perp A}(\bar{x}, q_T) &= M_A \int \frac{dp^+ d^2p db^-}{2(2\pi)^3} \int \frac{d^2k' d^2x d^2y}{(2\pi)^2} e^{-i(\underline{q}-\underline{k}') \cdot (\underline{x}-\underline{y})} \\ &\times \left\{ i x \underline{p} \cdot (\underline{x}-\underline{y}) A W_{unp}^{OAM} \left(p^+, \underline{p}, b^-, \frac{\underline{x}+\underline{y}}{2} \right) f_1^N(x, k'_T) \right. \\ &\left. - \frac{1}{m_N} \hat{z} \cdot (\underline{S} \times \underline{k}') W_{trans}^{symm} \left(p^+, \underline{p}, b^-, \frac{\underline{x}+\underline{y}}{2} \right) f_{1T}^{\perp N}(x, k'_T) \right\} S_{\underline{x}\underline{y}}[b^-, -\infty], \end{aligned} \quad (95)$$

where we have also interchanged $\underline{x} \leftrightarrow \underline{y}$ and $\underline{k}' \rightarrow -\underline{k}'$.

Eq. (95) is our main formal result for the DY Siverson function. We again see that the Siverson function in DY can arise through two distinct channels in this quasi-classical approach: the OAM channel that contains its preferred direction in the distribution W_{unp}^{OAM} and the transversity/Siverson density channel that generates its preferred direction through a local lensing mechanism $f_{1T}^{\perp N}$.

To demonstrate the importance of the Wilson lines for the Siverson function, for the moment, let us ignore the contribution of the Wilson lines associated with initial-state rescattering in Eq. (95). Without any such initial-state interactions, the nucleonic Siverson function is zero, $f_{1T}^N = 0$ [22, 48, 21], leaving

$$\begin{aligned} \hat{z} \cdot (\underline{J} \times \underline{q}) f_{1T}^{\perp A}(\bar{x}, q_T) &= M_A \int \frac{dp^+ d^2p db^-}{2(2\pi)^3} \int \frac{d^2k' d^2x d^2y}{(2\pi)^2} e^{-i(\underline{q}-\underline{k}') \cdot (\underline{x}-\underline{y})} \\ &\times i x \underline{p} \cdot (\underline{x}-\underline{y}) A W_{unp}^{OAM} \left(p^+, \underline{p}, b^-, \frac{\underline{x}+\underline{y}}{2} \right) f_1^N(x, k'_T) = 0, \end{aligned} \quad (96)$$

which vanishes after b^- integration because of the rotational and PT -symmetry conditions (B7).

4.2 Sign Reversal of the Siverson Function Between SIDIS and DY

Now that the DY Siverson function (95) is expressed in the same form as the Siverson function for SIDIS (57), we can compare both expressions to see how the nuclear Siverson functions have changed between SIDIS and DY and understand the origin of the SIDIS/DY sign-flip relation [11]

$$f_{1T}^{\perp A}(x, k_T) \Big|_{SIDIS} = -f_{1T}^{\perp A}(x, k_T) \Big|_{DY}. \quad (97)$$

First, we notice that the transversity/Siverson density channel (the second term in the curly brackets) has changed signs as required between (57) and (95). Mathematically, this occurs because of the $\underline{k}' \rightarrow -\underline{k}'$ interchange, simply because the momentum going into the Wilson line in SIDIS corresponds to the momentum coming from the Wilson line in DY (cf. Figs. 5 and 11). The transversity/Siverson density channel contribution thus automatically satisfies the sign-flip relation (97).

The OAM channel contribution to Eq. (95) is more subtle; although the prefactor has not changed as compared to Eq. (57), the longitudinal coordinate b^- integral entering (95) for DY can be modified using $b^- \rightarrow -b^-$ substitution along with Eq. (B7) to give

$$\int db^- W_{unp}^{OAM}(p, b) S_{\underline{x}\underline{y}}[b^-, -\infty] = - \int db^- W_{unp}^{OAM}(p, b) S_{\underline{x}\underline{y}}[-b^-, -\infty]. \quad (98)$$

When evaluating the dipole S -matrix we neglect the polarization effects as being energy suppressed. Therefore, for the purpose of this S -matrix, the nucleus has a rotational symmetry around the z -axis (see Fig. 6 for axes labels). We thus write

$$S_{\underline{x}\underline{y}}[-b^-, -\infty] \stackrel{PT}{=} S_{-\underline{x}, -\underline{y}}[+\infty, b^-] \stackrel{z\text{-rotation}}{=} S_{\underline{x}\underline{y}}[+\infty, b^-], \quad (99)$$

where z -rotation denotes a half-revolution around the z -axis. Using Eq. (99) in Eq. (98) we arrive at

$$\overbrace{\int db^- W_{unp}^{OAM}(p, b) S_{\underline{x}\underline{y}}[b^-, -\infty]}^{\text{DY}} = - \overbrace{\int db^- W_{unp}^{OAM}(p, b) S_{\underline{x}\underline{y}}[+\infty, b^-]}^{\text{SIDIS}}. \quad (100)$$

One can also simply see that Eq. (100) is true by using the quasi-classical GM/MV dipole S -matrix from Eq. (70) on its right-hand-side, along with

$$S_{\underline{x}\underline{y}}[b^-, -\infty] = \exp \left[-\frac{1}{4} |\underline{x} - \underline{y}|^2 Q_s^2 \left(\frac{\underline{x} + \underline{y}}{2} \right) \left(\frac{b^- + R^-}{2R^-} \right) \ln \frac{1}{|\underline{x} - \underline{y}| \Lambda} \right] \quad (101)$$

on its left-hand-side. We conclude that the OAM channel contributions to the SIDIS Siverson function (57) and the DY Siverson function (95) also satisfy the sign-flip relation (97).

Therefore, for any Wigner distribution $W(p, b)$, the Siverson functions at the quasi-classical level for SIDIS (57) and for DY (95) are equal in magnitude and opposite in sign, (97). This statement is a direct consequence of the invariance of $W(p, b)$ under rotations and PT -reversal, (B7), and it mirrors in this context the original derivation by Collins [11].

The advantage of our approach here, apart from providing the explicit formal results (57) and (95), is in the new physical interpretation of the transverse spin asymmetry in the OAM channel. As described in the Introduction following Fig. 1, the incoming antiquark is more likely to interact with the ‘‘front’’ of the nucleus, due to shadowing effects, thus scattering on the nucleon moving out of the page in Fig. 1. This is justified by the $S_{\underline{x}\underline{y}}[b^-, -\infty]$ function in Eq. (95) (see also (101)), which is largest for $b^- = -R^-$. Thus the virtual photon is produced preferentially out of the page; this leads to a non-zero STSA in DY. The sign reversal relation follows from comparing Figs. 1 and 2: in DY the particles are produced preferentially left-of-beam, while in SIDIS the produced hadrons come out mainly right-of-beam.

The rigid-rotator toy model of Sec. 3.3 can also be constructed for DY Siverson function. However, due to the sign-reversal relation (97) we can read off the answer for the DY Siverson function in the rigid-rotator model as being negative of that in Eq. (77) for moderate k_T and negative of Eq. (79) for $k_T \gg Q_s$. All the conclusions about the relative importance of the two contributing channels remain the same.

5 Discussion

The main goal of this work was to construct SIDIS and DY Sivers functions in the quasi-classical GM/MV approximation, which models a proton as a large nucleus, and which we modified by giving the nucleus a non-zero OAM. The main formal results are given in Eqs. (57) (SIDIS) and (95) (DY). We showed that there are two main mechanisms generating the quasi-classical Sivers function: the OAM channel and the transversity channel. The former is leading in saturation power counting; it also dominates for $k_T < Q_s/\sqrt{\alpha_s}$, that is both inside and, for $Q_s < k_T < Q_s/\sqrt{\alpha_s}$, outside of the saturation region. At higher k_T the transversity channel dominates. In the future our quasi-classical calculation can be augmented by including evolution corrections to the Sivers function, making the whole formalism ready for phenomenological applications, similar to the successful use of nonlinear small- x evolution equations [65, 66, 67, 68, 69, 70, 71] to description (and prediction) of high energy scattering data [72, 73].

Perhaps just as important, we constructed a novel physical mechanism of the STSA generation. This is the OAM channel. The OAM mechanism, while diagrammatically very similar to the original BHS mechanism [10], provides a different interpretation from the ‘lensing’ effect [10, 21] or the color-Lorentz force of [19, 18]. The OAM mechanism is described in the Introduction, in the discussion around Figs. 1 and 2. It is based on interpreting the extra rescattering proposed by BHS as a shadowing-type correction. The STSA is then generated by the combination of the OAM and shadowing. The shadowing makes sure the projectile interacts differently with the front and the back of the target, generating the asymmetry of the produced particles.

While shadowing is a high-energy phenomenon, and our calculation was done in the high-energy approximation $\hat{s} \gg \perp^2$ (though for $x \sim \mathcal{O}(1)$), it may be that the OAM mechanism for generating STSA is still valid for lower-energy scattering, though of course the formulas derived above would not apply in such regime. At lower energies the difference between the interactions of the projectile with the front/back of the target may result from, say, energy loss of the projectile as it traverses the target. Again, combined with the target rotation this would generate STSA, and, hence, the Sivers function. The formalism needed to describe such a low-energy process would be quite different from the one presented above; moreover, the correct degrees of freedom may not be quarks and gluons anymore. However, the main physics principle of combining OAM with the difference in interaction probabilities between the projectile and front/back of the target to generate STSA may be valid at all energies.

Returning to higher energies and the derived formulas (57) and (95), let us point out that these results, when applied to experimental data, may allow one to determine the distribution of intrinsic transverse momentum $\underline{p}(b, b^-)$ of partons in the hadronic or nuclear target, along with the transversity/Sivers function density in the target. This would complement the existing methods of spatial imaging of quarks and gluons inside the hadrons and nuclei [74], providing a new independent cross-check for those methods.

Acknowledgments

We would like to thank Daniel Boer, Dick Furnstahl, Leonard Gamberg and Feng Yuan for useful correspondence.

This research is sponsored in part by the U.S. Department of Energy under Grant No. de-sc0004286.

A Wigner Distributions with Multiple Rescatterings

The aim of this Appendix is to justify the result given in Eq. (23). To study the interplay between the local “knockout” channel of deep inelastic scattering and the coherent multiple rescattering on the nuclear remnants, it is illustrative to consider a minimal case with both features. This process, shown in Fig. 12, consists of the knockout sub-process followed by a single rescattering on a different quark from a second nucleon in the nucleus. Rescattering on a second nucleon receives a combinatoric enhancement of order $\sim A^{1/3}$ compared to rescattering on the same nucleon; the former is $\mathcal{O}(1)$ in the saturation power counting, while the latter is $\mathcal{O}(\alpha_s)$.

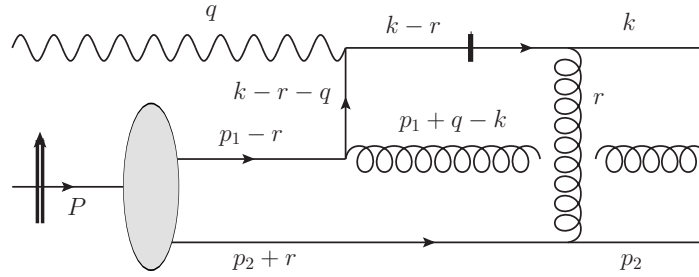


Figure 12: The minimal SIDIS process containing both the “knockout” of a quark from the nuclear wave function and rescattering on a different quark from a second nucleon. The short thick vertical line indicates that the pole of the intermediate quark propagator is picked up in the calculation.

The total SIDIS amplitude M_{tot} depicted in Fig. 12 consists of a loop integral connecting the mean-field single-particle wave functions $\psi(p)$ of the nucleus to a scattering amplitude M_{K+R} denoting both the “knockout” and rescattering processes:

$$M_{tot} = \int \frac{dr^+ d^2r}{2(2\pi)^3} \frac{P^+}{(p_1^+ - r^+)(p_2^+ + r^+)} \psi(p_1 - r) \psi(p_2 + r) M_{K+R}(p_1 - r, p_2 + r, q, k, r), \quad (\text{A1})$$

where a sum over spins and colors of the participating quarks is implied. Squaring both sides of (A1) and integrating out the final-state momenta p_1 and p_2 gives

$$\begin{aligned} \langle |M_{tot}|^2 \rangle &\equiv A(A-1) \int \frac{dp_1^+ d^2p_1 dp_2^+ d^2p_2}{[2(2\pi)^3]^2 (p_1^+ + q^+) p_2^+} |M_{tot}|^2 \\ &= \int \frac{dp_1^+ d^2p_1 dp_2^+ d^2p_2}{[2(2\pi)^3]^2 (p_1^+ + q^+) p_2^+} \frac{dr^+ d^2r dr'^+ d^2r'}{2(2\pi)^3 2(2\pi)^3} \frac{A(A-1)(P^+)^2}{\sqrt{(p_1^+ - r^+)(p_2^+ + r^+)(p_1^+ - r'^+)(p_2^+ + r'^+)}} \\ &\quad \times \int db_1^- d^2b_1 db_2^- d^2b_2 e^{-i(r-r') \cdot (b_1 - b_2)} W\left(p_1 - \frac{r+r'}{2}, b_1\right) W\left(p_2 + \frac{r+r'}{2}, b_2\right) \\ &\quad \times M_{K+R}(p_1 - r, p_2 + r, q, k, r) M_{K+R}^*(p_1 - r', p_2 + r', q, k, r'), \end{aligned} \quad (\text{A2})$$

where we have employed the Wigner distributions defined in Eq. (16) above and summed over all pairs of nucleons.

Eq. (A2) is still far from Eq. (23) because in (A2) we do not have the amplitude squared: instead we have the product of M_{K+R} and M_{K+R}^* with different arguments. It is easier to further analyze the expression separately for the transverse and longitudinal degrees of freedom. We proceed by taking the classical limits, in which case the Wigner distributions give us the position and momentum distributions of nucleons simultaneously. Moreover, for the large nucleus at hand the Wigner distributions depend on \underline{b}_1 and \underline{b}_2 weakly over the perturbatively short distances associated with the Feynman diagrams. We thus define $\underline{b} = (\underline{b}_1 + \underline{b}_2)/2$ and $\underline{\Delta}b = \underline{b}_1 - \underline{b}_2$ and write

$$\begin{aligned}
& \int d^2r d^2r' d^2b_1 d^2b_2 e^{i(\underline{r}-\underline{r}')\cdot(\underline{b}_1-\underline{b}_2)} W\left(p_1 - \frac{r+r'}{2}, b_1\right) W\left(p_2 + \frac{r+r'}{2}, b_2\right) \\
& \times M_{K+R}(p_1 - r, p_2 + r, q, k, r) M_{K+R}^*(p_1 - r', p_2 + r', q, k, r') \approx \int d^2r d^2r' d^2b d^2\Delta b e^{i(\underline{r}-\underline{r}')\cdot\underline{\Delta}b} \\
& \times W\left(p_1 - \frac{r+r'}{2}, b_1^-, \underline{b}\right) W\left(p_2 + \frac{r+r'}{2}, b_2^-, \underline{b}\right) M_{K+R}(p_1 - r, p_2 + r, q, k, r) \\
& \times M_{K+R}^*(p_1 - r', p_2 + r', q, k, r') = (2\pi)^2 \int d^2r d^2b W\left(p_1^+ - \frac{r^+ + r'^+}{2}, \underline{p}_1 - \underline{r}, b_1^-, \underline{b}\right) \\
& \times W\left(p_2^+ + \frac{r^+ + r'^+}{2}, \underline{p}_2 + \underline{r}, b_2^-, \underline{b}\right) M_{K+R}(p_1^+ - r^+, \underline{p}_1 - \underline{r}, p_2^+ + r^+, \underline{p}_2 + \underline{r}, q, k, r^+, \underline{r}) \\
& \times M_{K+R}^*(p_1^+ - r'^+, \underline{p}_1 - \underline{r}, p_2^+ + r'^+, \underline{p}_2 + \underline{r}, q, k, r'^+, \underline{r}). \tag{A3}
\end{aligned}$$

Now the difference in the arguments of M_{K+R} and M_{K+R}^* is only in the longitudinal momenta r^+ and r'^+ . To integrate over these momenta we notice that, as follows from Fig. 12, in the high energy kinematics at hand the leading contribution to the amplitude M_{K+R} comes from the region where $p_1^+, p_2^+ \gg r^+, r'^+$. In this regime we combine Eqs. (A2) and (A3) to write

$$\begin{aligned}
\langle |M_{tot}|^2 \rangle &= \int \frac{dp_1^+ d^2p_1 dp_2^+ d^2p_2}{[2(2\pi)^3]^2 (p_1^+ + q^+) p_2^+} \frac{dr^+ dr'^+ d^2r (P^+)^2}{4(2\pi)^4 p_1^+ p_2^+} db_1^- db_2^- d^2b e^{-i\frac{1}{2}(r^+ - r'^+)(b_1^- - b_2^-)} A(A-1) \\
& \times W\left(p_1^+, \underline{p}_1 - \underline{r}, b_1^-, \underline{b}\right) W\left(p_2^+, \underline{p}_2 + \underline{r}, b_2^-, \underline{b}\right) M_{K+R}(p_1^+, \underline{p}_1 - \underline{r}, p_2^+, \underline{p}_2 + \underline{r}, q, k, r^+, \underline{r}) \\
& \times M_{K+R}^*(p_1^+, \underline{p}_1 - \underline{r}, p_2^+, \underline{p}_2 + \underline{r}, q, k, r'^+, \underline{r}). \tag{A4}
\end{aligned}$$

In the $p_1^+, p_2^+ \gg r^+, r'^+$ kinematics the amplitude M_{K+R} contains only one pole in r^+ resulting from the denominator of the $k - r$ quark propagator (cf. [25, 63, 33]). We can thus write

$$M_{K+R}(p_1 - r, p_2 + r, q, k) = \frac{i}{(k - r)^2 + i\epsilon} \tilde{M}_{K+R}(p_1 - r, p_2 + r, q, k), \tag{A5}$$

where \tilde{M}_{K+R} denotes the rest of the diagram which does not contain singularities in r^+ in the $p_1^+, p_2^+ \gg r^+, r'^+$ approximation. (Note that \tilde{M}_{K+R} also contains the numerator of the $k - r$ quark propagator.) Since $(k - r)^2 \approx -k^- r^+ + \underline{k}^2 - (\underline{k} - \underline{r})^2$ we can use Eq. (A5) to integrate

over r^+ ,

$$\begin{aligned}
& \int_{-\infty}^{\infty} \frac{dr^+}{2\pi} e^{-i\frac{1}{2}r^+(b_1^- - b_2^-)} M_{K+R}(p_1 - r, p_2 + r, q, k) \\
& \approx \frac{1}{k^-} \theta(b_2^- - b_1^-) \tilde{M}_{K+R}(p_1^+, \underline{p}_1 - \underline{r}, p_2^+, \underline{p}_2 + \underline{r}, q, k) \\
& = \frac{1}{k^-} \theta(b_2^- - b_1^-) M_K(p_1 - r, q, k - r) M_R(p_2 + r, k - r, k, r). \tag{A6}
\end{aligned}$$

Here we assumed that $r^+ = [\underline{k}^2 - (\underline{k} - \underline{r})^2]/k^- \approx 0$ in our kinematics. After putting the $k - r$ quark propagator on mass shell the amplitude \tilde{M}_{K+R} factorizes into a product of separate amplitudes for knockout $M_K(p_1 - r, q, k - r)$ and rescattering $M_R(p_2 + r, k - r, k, r)$ [25, 63, 33], as employed in Eq. (A6), where the sum over quark polarizations and colors is implicit.

With the help of Eq. (A6) (and a similar one for the r'^+ -integration of M_{K+R}^*) we write

$$\begin{aligned}
\langle |M_{tot}|^2 \rangle &= \int \frac{dp_1^+ d^2p_1 dp_2^+ d^2p_2}{[2(2\pi)^3]^2 (p_1^+ + q^+) p_2^+} \frac{d^2r}{4(2\pi)^2} \frac{A(A-1)(P^+)^2}{p_1^+ p_2^+ (k^-)^2} db_1^- db_2^- d^2b \theta(b_1^- - b_2^-) \\
& \quad \times W(p_1^+, \underline{p}_1 - \underline{r}, b_1^-, \underline{b}) W(p_2^+, \underline{p}_2 + \underline{r}, b_2^-, \underline{b}) \\
& \quad \times |M_K(p_1 - r, q, k - r)|^2 |M_R(p_2 + r, k - r, k, r)|^2. \tag{A7}
\end{aligned}$$

Defining the energy-independent (at the quasi-classical level) rescattering amplitude by [25, 33]

$$|A_R(p_2 + r, k - r, k, r)|^2 \equiv \frac{1}{4(p_2^+)^2 (k^-)^2} |M_R(p_2 + r, k - r, k, r)|^2 \tag{A8}$$

and denoting the average of this object in the Wigner distribution by the angle brackets

$$\begin{aligned}
\langle |A_R(k, r)|^2 \rangle (b_1^-, \underline{b}) &= \int \frac{dp_2^+ d^2p_2 db_2^-}{2(2\pi)^3} \theta(b_2^- - b_1^-) (A-1) W(p_2^+, \underline{p}_2 + \underline{r}, b_2^-, \underline{b}) \\
& \quad \times |A_R(p_2 + r, k - r, k, r)|^2 \tag{A9}
\end{aligned}$$

we rewrite Eq. (A7) as

$$\begin{aligned}
\langle |M_{tot}|^2 \rangle &= A \int \frac{dp_1^+ d^2p_1 db_1^- d^2b}{2(2\pi)^3} \frac{(P^+)^2}{p_1^+ (p_1^+ + q^+)} W(p_1^+, \underline{p}_1, b_1^-, \underline{b}) \\
& \quad \times \int \frac{d^2r}{(2\pi)^2} |M_K(p_1, q, k - r)|^2 \langle |A_R(k, r)|^2 \rangle (b_1^-, \underline{b}). \tag{A10}
\end{aligned}$$

In arriving at Eq. (A10) we have shifted the momentum $p_1 \rightarrow p_1 + r$.

We now define the ‘‘energy-independent’’ total and ‘‘knockout’’ amplitudes [25, 33]

$$|A_{tot}|^2 \equiv \frac{1}{4(P^+)^2 (q^-)^2} |M_{tot}|^2, \quad |A_k|^2 \equiv \frac{1}{4(p_1^+)^2 (q^-)^2} |M_K|^2. \tag{A11}$$

Employing the Fourier transform (21) we reduce Eq. (A10) to

$$\begin{aligned} \langle |A_{tot}|^2 \rangle = & A \int \frac{dp_1^+ d^2 p_1 db_1^- d^2 b}{2(2\pi)^3} \frac{p_1^+}{p_1^+ + q^+} W(p_1^+, \underline{p}_1, b_1^-, \underline{b}) \int d^2 x d^2 y e^{-i \underline{k} \cdot (\underline{x} - \underline{y})} \\ & \times A_K(p_1, q, k^-, r^+, \underline{x} - \underline{b}) A_K^*(p_1, q, k^-, r^+, \underline{y} - \underline{b}) \langle |A_R|^2 \rangle(k^-, \underline{x} - \underline{y}, b_1^-, \underline{b}) \end{aligned} \quad (\text{A12})$$

with

$$\langle |A_R|^2 \rangle(k^-, \underline{x} - \underline{y}, b_1^-, \underline{b}) = \int \frac{d^2 r}{(2\pi)^2} e^{i \underline{r} \cdot (\underline{x} - \underline{y})} \langle |A_R(k, r)|^2 \rangle(b_1^-, \underline{b}). \quad (\text{A13})$$

Comparing Eq. (A10) to Eq. (22) we see that, just like in all high energy QCD scattering calculations [25, 33, 30, 31, 32] the rescattering can be factored out into a multiplicative factor in the transverse coordinate space. Similar to the above one can show that all further rescatterings would only introduce more multiplicative factors. Defining a somewhat abbreviated notation

$$\begin{aligned} A(p, q, \underline{x} - \underline{b}) A^*(p, q, \underline{y} - \underline{b}) \equiv & A_K(p, q, k^-, r^+, \underline{x} - \underline{b}) A_K^*(p, q, k^-, r^+, \underline{y} - \underline{b}) \\ & \times \langle |A_R|^2 \rangle(k^-, \underline{x} - \underline{y}, b_1^-, \underline{b}) \end{aligned} \quad (\text{A14})$$

we see that Eq. (A12) reduces to Eq. (23), as desired. The above discussion also demonstrates how multiple rescatterings factorize in the transverse coordinate space: in the high energy kinematics they are included through the Wilson lines of Eqs. (26) and (27). The Wilson line correlator $D_{\underline{x}\underline{y}}[+\infty, b^-]$ from (27) contains a b^- -ordered product of multiple rescattering factors $\langle |A_R|^2 \rangle$ from all the interacting nucleons [75, 63].

B The Role of PT -Symmetry

The decompositions (57) and (95) essentially break the Wilson line operator \mathcal{U} in the definition (2) into two parts: the coherent rescattering $S_{\underline{x}\underline{y}}[+\infty, b^-]$ on other spectator nucleons which is a leading-order contribution in the saturation power counting, and the subleading lensing interaction with the same nucleon which generates $f_{1T}^{\perp N}$. If we neglect the Wilson line operator \mathcal{U} entirely, then we know that the Sivers function of the nucleus $f_{1T}^{\perp A}$ must vanish, as first proved by Collins [15]. But if we drop $f_{1T}^{\perp N}$ and $S_{\underline{x}\underline{y}}[+\infty, b^-]$ from (57), we do not obviously get zero:

$$\begin{aligned} \hat{z} \cdot (\underline{J} \times \underline{k}) f_{1T}^{\perp A}(x, k_T) = & M_A A \int \frac{dp^+ d^2 p db^-}{2(2\pi)^3} d^2 x d^2 y \frac{d^2 k'}{(2\pi)^2} e^{-i(\underline{k} - \underline{k}') \cdot (\underline{x} - \underline{y})} \\ & \times i x \underline{p} \cdot (\underline{x} - \underline{y}) W_{unp}^{OAM} \left(p^+, \underline{p}, b^-, \frac{\underline{x} + \underline{y}}{2} \right) f_1^N(x, k'_T) \stackrel{?}{=} 0. \end{aligned} \quad (\text{B1})$$

The right-hand side of this equation must vanish for wave functions described by W_{unp}^{OAM} that are PT eigenstates [15]; we can see this explicitly by considering the constraints on $W_\sigma(p, b)$ due to rotational invariance and PT symmetry. It is most convenient to enumerate the rotational symmetry properties of the nucleon distribution $W_\sigma(p, b)$ in the rest frame of the nucleus, using a cylindrical vector basis coaxial to the transverse spin vector \underline{S} . This basis $(\hat{e}_\rho, \hat{e}_\theta, \hat{x})$ is shown in Fig. 13 and is defined by

$$\begin{pmatrix} \hat{e}_\rho \\ \hat{e}_\theta \end{pmatrix} = \begin{pmatrix} b_y/b_\rho & b_z/b_\rho \\ -b_z/b_\rho & b_y/b_\rho \end{pmatrix} \begin{pmatrix} \hat{y} \\ \hat{z} \end{pmatrix} = \begin{pmatrix} \cos \theta & \sin \theta \\ -\sin \theta & \cos \theta \end{pmatrix} \begin{pmatrix} \hat{y} \\ \hat{z} \end{pmatrix} \quad (\text{B2})$$

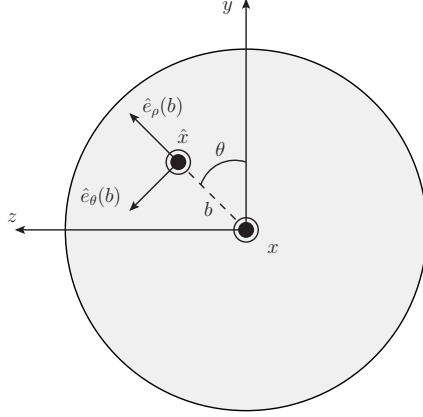


Figure 13: Definition of the cylindrical coordinate basis (B2) convenient for formulating the symmetry properties of the nucleonic distribution $W_\sigma(p, b)$ in the rest frame of the nucleus.

where $(p_\rho(b), p_\theta(b)) = p \cdot (\hat{e}_\rho(b), \hat{e}_\theta(b))$ and $b_\rho \equiv \sqrt{b_y^2 + b_z^2}$.

First, the distribution must be symmetric under rotations about the transverse spin S_x , which are easy to express in this cylindrical basis:

$$W_\sigma(p_x; p_\rho(b); p_\theta(b); b) = W_\sigma(p_x; p_\rho(b'); p_\theta(b'); b'). \quad (\text{B3})$$

Second, if the nucleus is in a PT -symmetric eigenstate of the QCD Hamiltonian, then $W_\sigma(p, b)$ should be invariant under PT transformations. These transformations reverse the coordinates ($b \rightarrow -b$) and pseudovectors like the spin ($S, \sigma \rightarrow -S, -\sigma$), but leave the momentum vector p unchanged. Using this transformation, together with rotational invariance as shown in Fig. 14 we obtain

$$\begin{aligned} W_\sigma(p_\rho(b), p_\theta(b), p_x; b; S_x) &\stackrel{PT}{=} W_{-\sigma}(p_\rho(b), p_\theta(b), p_x; -b; -S_x) \\ &= W_{-\sigma}(-p_\rho(-b), -p_\theta(-b), p_x; b; -S_x) \\ &\stackrel{R_b}{=} W_\sigma(-p_\rho(b), p_\theta(b), -p_x; b; S_x) \\ &\quad \vdots \end{aligned} \quad (\text{B4})$$

$$W_\sigma(p_\rho(b), p_\theta(b), p_x; b; S_x) = W_\sigma(-p_\rho(b), p_\theta(b), -p_x; b; S_x),$$

where the rotation R_b is a half-revolution in the Sb -plane. This means that in a PT eigenstate with transverse spin S_x , the only allowed direction of net momentum flow corresponds to the azimuthal orbital momentum p_θ and explains the naming convention W^{OAM} in (49).

The distributions that enter (57) and (95), however, are the (anti)symmetrized distributions under reversal of the transverse momenta ($p_x, p_y \rightarrow -p_x, -p_y$). For these purposes, it is more convenient to write the distribution $W_\sigma(p, b)$ in terms of the Cartesian basis

$$W(p_x, p_y, p_z; b) = W_\sigma\left(p_x; \frac{b_y}{b_\rho} p_\rho(b) - \frac{b_z}{b_\rho} p_\theta(b); \frac{b_z}{b_\rho} p_\rho(b) + \frac{b_y}{b_\rho} p_\theta(b); b\right). \quad (\text{B5})$$

Using the symmetry properties (B3) and (B4), we can write the \underline{p} -reversed distribution in terms

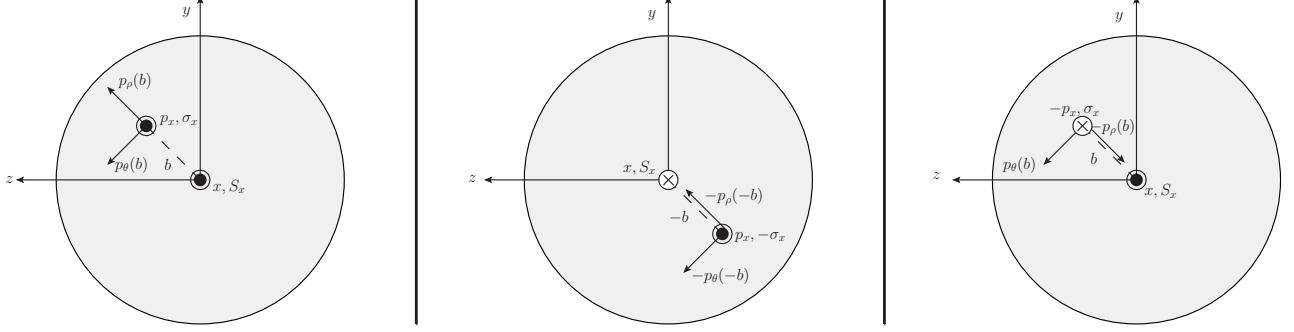


Figure 14: Illustration of the PT transformation and rotational symmetry in the rest frame used in (B4). Left panel: illustration of the momentum flow represented by $W_\sigma(p, b)$. Center panel: under a PT transformation, the spins S, σ and coordinate b are reversed, but the momentum p is invariant. Right panel: rotation of the center panel by π about the vector $\vec{S} \times \vec{b}$ returns the distribution to its original position b , with p_ρ and p_x having been reversed.

of the distribution at a point $\bar{b} \equiv (b_x, b_y, -b_z)$ on the opposite side of the nucleus:

$$\begin{aligned}
W_\sigma(-p_x, -p_y, p_z; b) &= W_\sigma \left(-p_x; -\frac{b_y}{b_\rho} p_\rho(b) + \frac{b_z}{b_\rho} p_\theta(b); \frac{b_z}{b_\rho} p_\rho(b) + \frac{b_y}{b_\rho} p_\theta(b); b \right) \\
&\stackrel{\text{Eq. (B3)}}{=} W_\sigma \left(-p_x; -\frac{b_y}{b_\rho} p_\rho(\bar{b}) - \frac{b_z}{b_\rho} p_\theta(\bar{b}); -\frac{b_z}{b_\rho} p_\rho(\bar{b}) + \frac{b_y}{b_\rho} p_\theta(\bar{b}); \bar{b} \right) \\
&\stackrel{\text{Eq. (B4)}}{=} W_\sigma \left(p_x; \frac{b_y}{b_\rho} p_\rho(\bar{b}) - \frac{b_z}{b_\rho} p_\theta(\bar{b}); \frac{b_z}{b_\rho} p_\rho(\bar{b}) + \frac{b_y}{b_\rho} p_\theta(\bar{b}); \bar{b} \right) \\
&= W_\sigma(p_x, p_y, p_z; \bar{b})
\end{aligned} \tag{B6}$$

\therefore

$$W_\sigma(-p_x, -p_y, p_z; b) = W_\sigma(p_x, p_y, p_z; \bar{b}).$$

Thus a nucleon on the back side of the nucleus has an opposite transverse momentum to a corresponding nucleon in the front of the nucleus. Therefore, the (anti)symmetrized distributions have definite parity under $b_z \rightarrow -b_z$:

$$\begin{aligned}
W_\sigma^{symm}(p, b) &\equiv \frac{1}{2} [W_\sigma(p, b) + (\underline{p} \rightarrow -\underline{p})] = +W_\sigma^{symm}(p, \bar{b}) \\
W_\sigma^{OAM}(p, b) &\equiv \frac{1}{2} [W_\sigma(p, b) - (\underline{p} \rightarrow -\underline{p})] = -W_\sigma^{OAM}(p, \bar{b}).
\end{aligned} \tag{B7}$$

Eq. (B7) tells us that a consequence of PT invariance in the nucleus is that the orbital angular momentum encountered at any point in the front of the nucleus is compensated by an equal and opposite orbital angular momentum from a corresponding point on the back of the nucleus. This is the resolution to the apparent paradox (B1): when we neglect all Wilson line contributions (both $S_{\underline{xy}}[+\infty, b^-]$ and $f_{1T}^{\perp N}$), the net asymmetry in the quark distribution is zero since $\int db^- W_{unp}^{OAM}(p, b) = 0$. Hence neglecting all Wilson line contributions yields zero Siverts function, consistent with [15].

An essential role is played in (57), then, by the rescattering factor $S_{\underline{xy}}[+\infty, b^-]$. In the OAM channel, even though the rescattering $S_{\underline{xy}}[+\infty, b^-]$ is not the source of a preferred transverse

direction, without it the net contribution to the Sivers function from OAM would vanish after integration over b^- , as can be gleaned from the left panel in Fig. 7. The rescattering factor $S_{xy}[+\infty, b^-]$ is essential because it introduces shadowing that breaks this front-back symmetry by screening quarks ejected from the front of the nucleus more than those ejected the back. The Sivers function relevant for SIDIS is therefore more sensitive to OAM from the back of the nucleus than from the front, which prevents the complete cancellation of the OAM contribution as in (B1).

This analysis is strikingly similar to the arguments that historically established the existence of the Sivers function. As Collins argued in [15], PT -invariance of any hadronic eigenstate prohibits a preferred direction that can generate the Sivers function. This is directly reflected in the vanishing of (B1) without the effects of multiple rescattering. And as Brodsky, Hwang, and Schmidt demonstrated in [10], the rescattering represented by the semi-infinite Wilson lines breaks this symmetry and permits a preferred direction for the asymmetry. Unlike that calculation, however, here the rescattering does not occur as color-correlated “lensing” due to rescattering on the remnants of the active quark. Here the interaction is explicitly color-decorrelated because the rescattering occurs on many nucleons whose colors are not correlated. Despite this difference, the rescattering effects are still sufficient to break the front-back symmetry and give rise to a net preferred direction for the asymmetry.

References

- [1] J. C. Collins, D. E. Soper, and G. F. Sterman, *Factorization of Hard Processes in QCD*, *Adv.Ser.Direct.High Energy Phys.* **5** (1988) 1–91, [hep-ph/0409313].
- [2] J. C. Collins and D. E. Soper, *Back-To-Back Jets in QCD*, *Nucl.Phys.* **B193** (1981) 381.
- [3] D. W. Sivers, *Single Spin Production Asymmetries from the Hard Scattering of Point-Like Constituents*, *Phys.Rev.* **D41** (1990) 83.
- [4] D. W. Sivers, *Hard scattering scaling laws for single spin production asymmetries*, *Phys.Rev.* **D43** (1991) 261–263.
- [5] A. Efremov and O. Teryaev, *On spin effects in Quantum Chromodynamics*, *Sov.J.Nucl.Phys.* **36** (1982) 140.
- [6] A. Efremov and O. Teryaev, *QCD Asymmetry and Polarized Hadron Structure Functions*, *Phys.Lett.* **B150** (1985) 383.
- [7] J.-w. Qiu and G. F. Sterman, *Single transverse spin asymmetries*, *Phys.Rev.Lett.* **67** (1991) 2264–2267.
- [8] X.-D. Ji, *Gluon correlations in the transversely polarized nucleon*, *Phys.Lett.* **B289** (1992) 137–142.
- [9] J.-w. Qiu and G. F. Sterman, *Single transverse spin asymmetries in hadronic pion production*, *Phys.Rev.* **D59** (1998) 014004, [hep-ph/9806356].

- [10] S. J. Brodsky, D. S. Hwang, and I. Schmidt, *Final state interactions and single spin asymmetries in semiinclusive deep inelastic scattering*, *Phys.Lett.* **B530** (2002) 99–107, [[hep-ph/0201296](#)].
- [11] J. C. Collins, *Leading twist single transverse-spin asymmetries: Drell-Yan and deep inelastic scattering*, *Phys.Lett.* **B536** (2002) 43–48, [[hep-ph/0204004](#)].
- [12] Y. Koike and S. Yoshida, *Probing the three-gluon correlation functions by the single spin asymmetry in $p^\uparrow p \rightarrow DX$* , *Phys.Rev.* **D84** (2011) 014026, [[arXiv:1104.3943](#)].
- [13] Y. Kanazawa and Y. Koike, *Chiral odd contribution to single transverse spin asymmetry in hadronic pion production*, *Phys.Lett.* **B478** (2000) 121–126, [[hep-ph/0001021](#)].
- [14] Y. Kanazawa and Y. Koike, *Estimate of a chiral odd contribution to single transverse spin asymmetry in hadronic pion production*, *Phys.Lett.* **B490** (2000) 99–105, [[hep-ph/0007272](#)].
- [15] J. C. Collins, *Fragmentation of transversely polarized quarks probed in transverse momentum distributions*, *Nucl.Phys.* **B396** (1993) 161–182, [[hep-ph/9208213](#)].
- [16] G. L. Kane, J. Pumplin, and W. Repko, *Transverse Quark Polarization in Large $p(T)$ Reactions, $e^+ e^-$ Jets, and Leptoproduction: A Test of QCD*, *Phys.Rev.Lett.* **41** (1978) 1689.
- [17] Y. V. Kovchegov and M. D. Sievert, *A New Mechanism for Generating a Single Transverse Spin Asymmetry*, *Phys.Rev.* **D86** (2012) 034028, [[arXiv:1201.5890](#)].
- [18] M. Burkardt, *Transverse Force on Quarks in DIS*, [arXiv:0810.3589](#).
- [19] M. Burkardt, *Transverse (Spin) Structure of Hadrons*, *PoS LC2010* (2010) 051, [[arXiv:1011.2220](#)].
- [20] A. V. Belitsky, X. Ji, and F. Yuan, *Final state interactions and gauge invariant parton distributions*, *Nucl.Phys.* **B656** (2003) 165–198, [[hep-ph/0208038](#)].
- [21] S. J. Brodsky, D. S. Hwang, Y. V. Kovchegov, I. Schmidt, and M. D. Sievert, *Single-Spin Asymmetries in Semi-inclusive Deep Inelastic Scattering and Drell-Yan Processes*, *Phys.Rev.* **D88** (2013) 014032, [[arXiv:1304.5237](#)].
- [22] S. J. Brodsky, D. S. Hwang, and I. Schmidt, *Initial state interactions and single spin asymmetries in Drell-Yan processes*, *Nucl.Phys.* **B642** (2002) 344–356, [[hep-ph/0206259](#)].
- [23] L. Gamberg and M. Schlegel, *Final state interactions and the Sivers function*, *AIP Conf.Proc.* **1374** (2011) 309–313, [[arXiv:1012.3395](#)].
- [24] L. Gamberg and M. Schlegel, *Final state interactions and the transverse structure of the pion using non-perturbative eikonal methods*, *Phys.Lett.* **B685** (2010) 95–103, [[arXiv:0911.1964](#)].

- [25] A. H. Mueller, *Small x Behavior and Parton Saturation: A QCD Model*, *Nucl. Phys.* **B335** (1990) 115.
- [26] L. D. McLerran and R. Venugopalan, *Gluon distribution functions for very large nuclei at small transverse momentum*, *Phys. Rev.* **D49** (1994) 3352–3355, [[hep-ph/9311205](#)].
- [27] L. D. McLerran and R. Venugopalan, *Green’s functions in the color field of a large nucleus*, *Phys. Rev.* **D50** (1994) 2225–2233, [[hep-ph/9402335](#)].
- [28] L. D. McLerran and R. Venugopalan, *Computing quark and gluon distribution functions for very large nuclei*, *Phys. Rev.* **D49** (1994) 2233–2241, [[hep-ph/9309289](#)].
- [29] E. Iancu and R. Venugopalan, *The color glass condensate and high energy scattering in QCD*, [hep-ph/0303204](#).
- [30] H. Weigert, *Evolution at small x_{bj} : The Color Glass Condensate*, *Prog. Part. Nucl. Phys.* **55** (2005) 461–565, [[hep-ph/0501087](#)].
- [31] J. Jalilian-Marian and Y. V. Kovchegov, *Saturation physics and deuteron gold collisions at RHIC*, *Prog. Part. Nucl. Phys.* **56** (2006) 104–231, [[hep-ph/0505052](#)].
- [32] F. Gelis, E. Iancu, J. Jalilian-Marian, and R. Venugopalan, *The Color Glass Condensate*, *Ann.Rev.Nucl.Part.Sci.* **60** (2010) 463–489, [[arXiv:1002.0333](#)].
- [33] Y. V. Kovchegov and E. Levin, *Quantum Chromodynamics at High Energy*. Cambridge University Press, 2012.
- [34] Y. V. Kovchegov, *Quantum structure of the non-Abelian Weizsäcker-Williams field for a very large nucleus*, *Phys. Rev.* **D55** (1997) 5445–5455, [[hep-ph/9701229](#)].
- [35] D. Boer, A. Dumitru, and A. Hayashigaki, *Single transverse-spin asymmetries in forward pion production at high energy: Incorporating small- x effects in the target*, *Phys.Rev.* **D74** (2006) 074018, [[hep-ph/0609083](#)].
- [36] D. Boer, A. Utermann, and E. Wessels, *The Saturation scale and its x -dependence from Lambda polarization studies*, *Phys.Lett.* **B671** (2009) 91–98, [[arXiv:0811.0998](#)].
- [37] D. Boer and A. Dumitru, *Polarized hyperons from pA scattering in the gluon saturation regime*, *Phys.Lett.* **B556** (2003) 33–40, [[hep-ph/0212260](#)].
- [38] F. Dominguez, J.-W. Qiu, B.-W. Xiao, and F. Yuan, *On the linearly polarized gluon distributions in the color dipole model*, *Phys.Rev.* **D85** (2012) 045003, [[arXiv:1109.6293](#)].
- [39] A. Metz and J. Zhou, *Distribution of linearly polarized gluons inside a large nucleus*, *Phys.Rev.* **D84** (2011) 051503, [[arXiv:1105.1991](#)].
- [40] Z.-B. Kang and F. Yuan, *Single Spin Asymmetry Scaling in the Forward Rapidity Region at RHIC*, *Phys.Rev.* **D84** (2011) 034019, [[arXiv:1106.1375](#)].

- [41] Z.-B. Kang and B.-W. Xiao, *Sivers asymmetry of Drell-Yan production in small- x regime*, *Phys.Rev.* **D87** (2013) 034038, [[arXiv:1212.4809](#)].
- [42] K. Golec-Biernat and M. Wüsthoff, *Saturation effects in deep inelastic scattering at low Q^2 and its implications on diffraction*, *Phys. Rev.* **D59** (1998) 014017, [[hep-ph/9807513](#)].
- [43] K. Golec-Biernat and M. Wüsthoff, *Saturation in diffractive deep inelastic scattering*, *Phys. Rev.* **D60** (1999) 114023, [[hep-ph/9903358](#)].
- [44] H. Kowalski and D. Teaney, *An impact parameter dipole saturation model*, *Phys. Rev.* **D68** (2003) 114005, [[hep-ph/0304189](#)].
- [45] P. Tribedy and R. Venugopalan, *Saturation models of HERA DIS data and inclusive hadron distributions in $p+p$ collisions at the LHC*, *Nucl.Phys.* **A850** (2011) 136–156, [[arXiv:1011.1895](#)].
- [46] T. Chou and C. N. Yang, *Hadronic Matter Current Distribution Inside a Polarized Nucleus and a Polarized Hadron*, *Nucl.Phys.* **B107** (1976) 1.
- [47] D. Boer, L. Gamberg, B. Musch, and A. Prokudin, *Bessel-Weighted Asymmetries in Semi Inclusive Deep Inelastic Scattering*, *JHEP* **1110** (2011) 021, [[arXiv:1107.5294](#)].
- [48] D. Boer, S. J. Brodsky, and D. S. Hwang, *Initial state interactions in the unpolarized Drell-Yan process*, *Phys.Rev.* **D67** (2003) 054003, [[hep-ph/0211110](#)].
- [49] D. Boer and P. Mulders, *Time reversal odd distribution functions in leptonproduction*, *Phys.Rev.* **D57** (1998) 5780–5786, [[hep-ph/9711485](#)].
- [50] G. P. Lepage and S. J. Brodsky, *Exclusive processes in perturbative quantum chromodynamics*, *Phys. Rev.* **D22** (1980) 2157.
- [51] S. J. Brodsky, G. P. Lepage, and P. B. Mackenzie, *On the elimination of scale ambiguities in perturbative quantum chromodynamics*, *Phys. Rev.* **D28** (1983) 228.
- [52] L. Lukaszuk and B. Nicolescu, *A Possible interpretation of $p p$ rising total cross-sections*, *Lett.Nuovo Cim.* **8** (1973) 405–413.
- [53] B. Nicolescu, *The Odderon today, Presented at the Moriond 1990 Conference* (1990).
- [54] C. Ewerz, *The Odderon in quantum chromodynamics*, [hep-ph/0306137](#).
- [55] J. Bartels, L. Lipatov, and G. Vacca, *A New odderon solution in perturbative QCD*, *Phys.Lett.* **B477** (2000) 178–186, [[hep-ph/9912423](#)].
- [56] Y. V. Kovchegov, L. Szymanowski, and S. Wallon, *Perturbative odderon in the dipole model*, *Phys.Lett.* **B586** (2004) 267–281, [[hep-ph/0309281](#)]. Dedicated to the memory of Jan Kwiecinski.
- [57] Y. Hatta, E. Iancu, K. Itakura, and L. McLerran, *Odderon in the color glass condensate*, *Nucl.Phys.* **A760** (2005) 172–207, [[hep-ph/0501171](#)].

- [58] A. Kovner and M. Lublinsky, *Odderon and seven Pomerons: QCD Reggeon field theory from JIMWLK evolution*, *JHEP* **0702** (2007) 058, [hep-ph/0512316].
- [59] S. Jeon and R. Venugopalan, *A Classical Odderon in QCD at high energies*, *Phys.Rev.* **D71** (2005) 125003, [hep-ph/0503219].
- [60] A. Bacchetta, M. Boglione, A. Henneman, and P. Mulders, *Bounds on transverse momentum dependent distribution and fragmentation functions*, *Phys.Rev.Lett.* **85** (2000) 712–715, [hep-ph/9912490].
- [61] A. Bacchetta and P. Mulders, *Deep inelastic leptonproduction of spin-one hadrons*, *Phys.Rev.* **D62** (2000) 114004, [hep-ph/0007120].
- [62] K. Itakura, Y. V. Kovchegov, L. McLerran, and D. Teaney, *Baryon stopping and valence quark distribution at small x* , *Nucl. Phys.* **A730** (2004) 160–190, [hep-ph/0305332].
- [63] Y. V. Kovchegov and A. H. Mueller, *Gluon production in current nucleus and nucleon nucleus collisions in a quasi-classical approximation*, *Nucl. Phys.* **B529** (1998) 451–479, [hep-ph/9802440].
- [64] B. Kopeliovich, J. Raufeisen, A. Tarasov, and M. Johnson, *Nuclear effects in the Drell-Yan process at very high-energies*, *Phys.Rev.* **C67** (2003) 014903, [hep-ph/0110221].
- [65] I. Balitsky, *Operator expansion for high-energy scattering*, *Nucl. Phys.* **B463** (1996) 99–160, [hep-ph/9509348].
- [66] Y. V. Kovchegov, *Small- x F_2 structure function of a nucleus including multiple pomeron exchanges*, *Phys. Rev.* **D60** (1999) 034008, [hep-ph/9901281].
- [67] J. Jalilian-Marian, A. Kovner, and H. Weigert, *The Wilson renormalization group for low x physics: Gluon evolution at finite parton density*, *Phys. Rev.* **D59** (1998) 014015, [hep-ph/9709432].
- [68] E. Iancu, A. Leonidov, and L. D. McLerran, *Nonlinear gluon evolution in the color glass condensate. I*, *Nucl. Phys.* **A692** (2001) 583–645, [hep-ph/0011241].
- [69] I. I. Balitsky, *Quark Contribution to the Small- x Evolution of Color Dipole*, *Phys. Rev. D* **75** (2007) 014001, [hep-ph/0609105].
- [70] E. Gardi, J. Kuokkanen, K. Rummukainen, and H. Weigert, *Running coupling and power corrections in nonlinear evolution at the high-energy limit*, *Nucl. Phys.* **A784** (2007) 282–340, [hep-ph/0609087].
- [71] Y. Kovchegov and H. Weigert, *Triumvirate of Running Couplings in Small- x Evolution*, *Nucl. Phys.* **A 784** (2007) 188–226, [hep-ph/0609090].
- [72] J. L. Albacete, N. Armesto, J. G. Milhano, P. Quiroga-Arias, and C. A. Salgado, *AAMQS: A non-linear QCD analysis of new HERA data at small- x including heavy quarks*, *Eur. Phys. J.* **C71** (2011) 1705, [arXiv:1012.4408].

- [73] J. L. Albacete and A. Dumitru, *A model for gluon production in heavy-ion collisions at the LHC with rcBK unintegrated gluon densities*, [arXiv:1011.5161](#).
- [74] A. Accardi, J. Albacete, M. Anselmino, N. Armesto, E. Aschenauer, *et. al.*, *Electron Ion Collider: The Next QCD Frontier - Understanding the glue that binds us all*, [arXiv:1212.1701](#).
- [75] J. Jalilian-Marian, A. Kovner, L. D. McLerran, and H. Weigert, *The intrinsic glue distribution at very small x* , *Phys. Rev.* **D55** (1997) 5414–5428, [[hep-ph/9606337](#)].